POWDER METALLURGICAL PROCESSING OF CHROMIUM CONTAINING IRON-ALUMINIUM POWDER PREPARED BY MECHANICAL ALLOYI

A Thesis Submitted
In Partial fulfilment of the Requirements
for the Degree of

MASTER OF TECHNOLOGY

by

INDRA KUMAR DIXIT

to the

DEPARTMENT OF MATERIALS AND METALLURGICAL ENGINEERING
INDIAN INSTITUTE OF TECHNOLOGY, KANPUR

JUNE 1996

CERTIFICATE

This is to certify that the thesis entitled, **P**

METALLURGICAL PROCESSING OF CHROMIUM CONTAINING IRON - ALUM

POWDER PREPARED BY MECHANICAL ALLOYING, is the record of the

carried out by **INDRA KUMAR DIXIT** under our supervision and ha

been submitted else where for the award of a degree.

R.K. Dube

(Prof. R. K. Dube)

S.Bhargava

Prof.S. Bharga

Department of Materials and Metallurgical Engine

Indian Institute of Technology

Kanpur

June, 1996

ACKNOWLEDGEMENTS

I wish to express my deep sense of indebtness and gratit to Prof. R.K. Dube and Prof. S. Bhargava for offering opportunity to work with them whose inspiring guidance, advice affectionate treatment has made this work possible. I felt th helping hands with me throughout the work without which progress would have been impossible. I salute them in reverence

I would like to express my special thanks to my friend Sanjeev, Piyush and Neeraj who made me believe that there is limit of being helpful. I also thank to Mr. Satyam Suwas and M Shantanu Das for his invaluable suggestions and help during stay at IIT Kanpur.

I also express my sincere thanks to Mr. B. Sharma, Mr.M. Mangole, Mr.K.P. Mukherji, Mr.S.C. Soni, Mr.Pal, Mr. Uma Shank Singh and all other technical staff for their assistance various stages of my work.

Thanks to all my unforgettable friends whose company ar affection I got during my stay at IIT Kanpur.

Indra Kumar Dixit

June, 1996

CONTENTS

LIST OF FIGURES

LIST OF TABLES

ABSTRACT

Iron aluminides based on Fe_3Al ordered intermetallics are currently being developed into a class of new inexpensive elevated temperature structural materials owing to their low density, high strength, reasonable ductility and excellent oxidation and sulfidation resistance. A number of processing methods have been used for fabrication of intermetallics. In recent studies, much attention has been paid to powder metallurgy processing because of the advantages in controlling microstructure, improving properties, and obtaining near net shape products.

In the present study, mechanical alloying of a mixture of Fe,Al and Cr elemental powders corresponding to Fe-28at%Al-5at%Cr and the subsequent powder metallurgical processing of mechanically alloyed powder via two routes were studied.

The mechanical alloying was performed in a high energy mechanical attritor for the mixture of Fe-Al-Cr powder for 80 hrs.The progress of mechanical alloying was studied by characterisation of powder samples taken out after different intervals of time. Mechanical alloying was found to produce a solid solution of Al in Fe and nanometer crytallite size of the powder.Lattice strain was also found to increase with milling time.

Powder metallurgical processing of mechanically alloyed powder was done via two routes. First route involved cold compaction of mechanically alloyed powder and its subsequent sintering and hot rolling. The second route involved hot pressing of mechanically alloyed powder. The density and mechanical properties of compacts made via hot pressing route was found to be superior to those prepared by cold compaction and sintering route.

INTRODUCTION

1.1 INTERMETALLIC COMPOUNDS: A GENERAL SURVEY

The search for high strength, high temperature materials has been continuous throughout the history of material science. For example, the demand for enhanced efficiency and performance of jet engines demands for high gas turbine combustion temperature, which has necessitated the development of materials that would withstand high temperatures and at the same time retain dimensional stability and resistance to surface attack. Also, for better performance, the jet engine require materials of low density and high temperature stability, thereby increasing thrust to weight ratio and engine efficiency.

This search for new high temperature structural materials has stimulated much interest in ordered intermetallics. Intermetallic compounds are phases which occur in the central part of the phase diagram between two or more metals with a characteristic crystal structure, and may have a very specific composition or a range of compositions. Because of the strong attraction between the unlike atoms involved, there is a strong preference in the selection of nearest neighbours which in turn can lead to an ordered structure, a high resistance to deformation (movement of lattice defects), and a high melting point. The high melting point in combination with the difficulty of movement of lattice defects leads to high strength and retention of strength to elevated temperatures.

However, these same features lead to "achilles heel" of th intermetallics, that of very low ductility (brittleness or lack c forgiveness) at room temperature. Thus, the major thrust in th development of usable intermetallics has been to "build-in reliability while maintaining attractive elevated temperatur properties. This has been achieved to an extent usin chemistry/processing/microstructure control and by use o composite concepts in which a reinforcing phase is incorporate into the intermetallic matrix to increase strength/stiffness an to deflect crack propagation (increase toughness).

Ordered intermetallic alloys can be divided into severa groups, e.g. Aluminides (e.g. Nickel, Iron & Titanium aluminides) Silicides (e.g. Cr_3Si, $TiSi_2$, Ni_3Si etc.), Trialuminides (e.g Al_3X where X is usually Ti, Zr, Hf, V, Nb or Ta), Beryllides (e.g $NbBe_{12}$), Chromides (e.g. Cr_2 Ti) etc.

Among these, nickel, iron and titanium aluminides have beer the focus of much of the research in recent years. These aluminides possess many attributes that make them attractive for high temperature structural applications (Table1.1). They contain enough aluminium to form, in oxidising environments, thin films of aluminium oxide (Al_2O_3) that often are compact and protective. They have low densities, relatively high melting points, and good high temperature strength properties (Table1.2). But like other ordered intermetallics, they also exhibit brittle fracture and low ductility at ambient temperatures. Poor fracture resistance and limited fabricability restrict the use of aluminides as engineering materials.[1-4] In recent years, alloying and processing have been employed to control the ordered crystal

Table 1.1

Applications of Structured Intermetallics.

Ni_3Al	- Diesel-engine turbocharger rotors;
	- high temperature dies and molds;
	- air craft parts;
	- turbine blades;
	- hydro turbines;
Fe_3Al	- Toasters, stoves, ovens;
	- automotive gas-turbine engines;
	- coal-gasification systems;
	- insulating wrappings for investment casting;
	- components needing high-temperature sulfidation;
Ti_3Al	- Transition duct support;
	- seal housing;
	- compressor sturters;
	- turbine frames;
	- LP turbine airfoils.

Table 1.2

Important Aluminides and Their Relevant Properties

Alloy	Crystal Structure	Melting point (^{o}C)	Density (gm/cm^3)	Yield Strength (MPa)	Young's Modulus ($x10^3 MPa$)
Ni_3Al	$L1_2$ (ordered fcc)	1390	7.5	250-300	178.6
NiAl	B2 (ordered bcc)	1640	5.9	250-475	294.4
Fe_3Al	DO_3 (ordered bcc)	1540	6.7	385-392	140.7
FeAl	B2 (ordered bcc)	1250	5.6	360-380	260.6
Ti_3Al	DO_{19} (ordered hcp)	1600	4.2	700-990	144.8
TiAl	$L1_o$ (ordered Tetragonal)	1460	3.9	400-650	175.8

structure, microstructural features, and grain boundary structure and composition to overcome the brittleness problem in ordere intermetallics.

1.2 IRON-ALUMINIDE

Iron aluminides based on Fe_3Al and FeAl are candidates for variety of structural applications. The combination of lo density, excellent oxidation and sulfidation resistance, and lac of strategic alloying elements makes these alloys particularl attractive. However, the major drawbacks of the iron aluminide are their low ductility and fracture toughness at ambient temperatures and their poor strength at temperatures above 600°C. Recently, considerable efforts have been devoted in improvin their mechanical properties through control of grain structures, alloy additions and material processing.

1.2.1 Fe-Al System

A number of investigations have been done on the Fe-Al syste by means of resistivity measurement, x-ray diffraction and electron microscopy.[5,6]

The Fe-Al system is characterised by a wide α-Fe solid solution range. The system entails five stable phases, namely Fe_3Al. FeAl, $FeAl_2$, Fe_2Al_5 and $FeAl_3$, each of them with a homogeneity range. Fe_3Al which has a DO_3 ordered superlattice structure is a low temperature phase. It is formed at 552°C and 26.5 at % Al by a first order reaction from FeAl (α_2). FeAl has a B2 ordered superlattice structure. It is formed at 1,310°C by a peritectic reaction corresponding to:

$$L(50.7at\%\ Al) + \alpha\text{-}Fe(45.2at\%\ Al) = FeAl(\alpha_2)$$

In Fig. 1.1 the formation of α_2(FeAl) is not shown as a peritecti reaction, but as a second order type reaction concordant with th Fe-Si and Fe-Ga system. $FeAl_2$ is formed by a peritectoida reaction at about 1,153°C and crystallises in a comple: rhombohedral structure. There is general agreement about th congruent formation of Fe_2Al_5. The melting point o: stoichiometric Fe_2Al_5 is 1,171°C. The Al-richest phase $FeAl_3$ i: formed peritectically at 1,157°C and crystallises in a monoclini structure.

The stable phases of interest are Fe_3Al and FeAl which have DO_3 and B2 ordered superlattice structures respectively. Both of these crystal structures (Fig.1.2)[1] are derivatives of BCC structures existing at room temperature over a range of 18 at % to nearly 36 at % Al and 36 at % to 50 at % Al respectively. The ordered DO_3 structure consists of eight bcc cells with each unit cell consisting of a total of sixteen atoms. Out of 16 atoms, 4 atoms are of Al at (3/4, 3/4, 3/4), (3,4, 1/4, 1/4), (1/4, 3/4, 1/4) and (1/4, 1/4, 3/4) lattice sites and remaining sites are occupied by 12 Fe atoms. B2 structure, on the other hand, has two interpenetrating simple cubic lattice with the atoms of each constituent at the body centre of the other. Thus, iron atoms at (0,0,0) and aluminium at (1/2,1/2,1/2) lattice sites.

1.2.2 Structural Defects in Ordered Fe-Al Intermetallics

Ho and Dodd[7] proposed that, as for NiAl and CoAl, antistructural vacancies appear to form on Fe sites in FeAl at Al contents > 50%. Vacancies may be formed in the iron aluminides by quenching from high temperature. Field ion microscopy showed that Fe-49.5% Al quenched from 1273 K contained a high (1.85 ± .05at%)

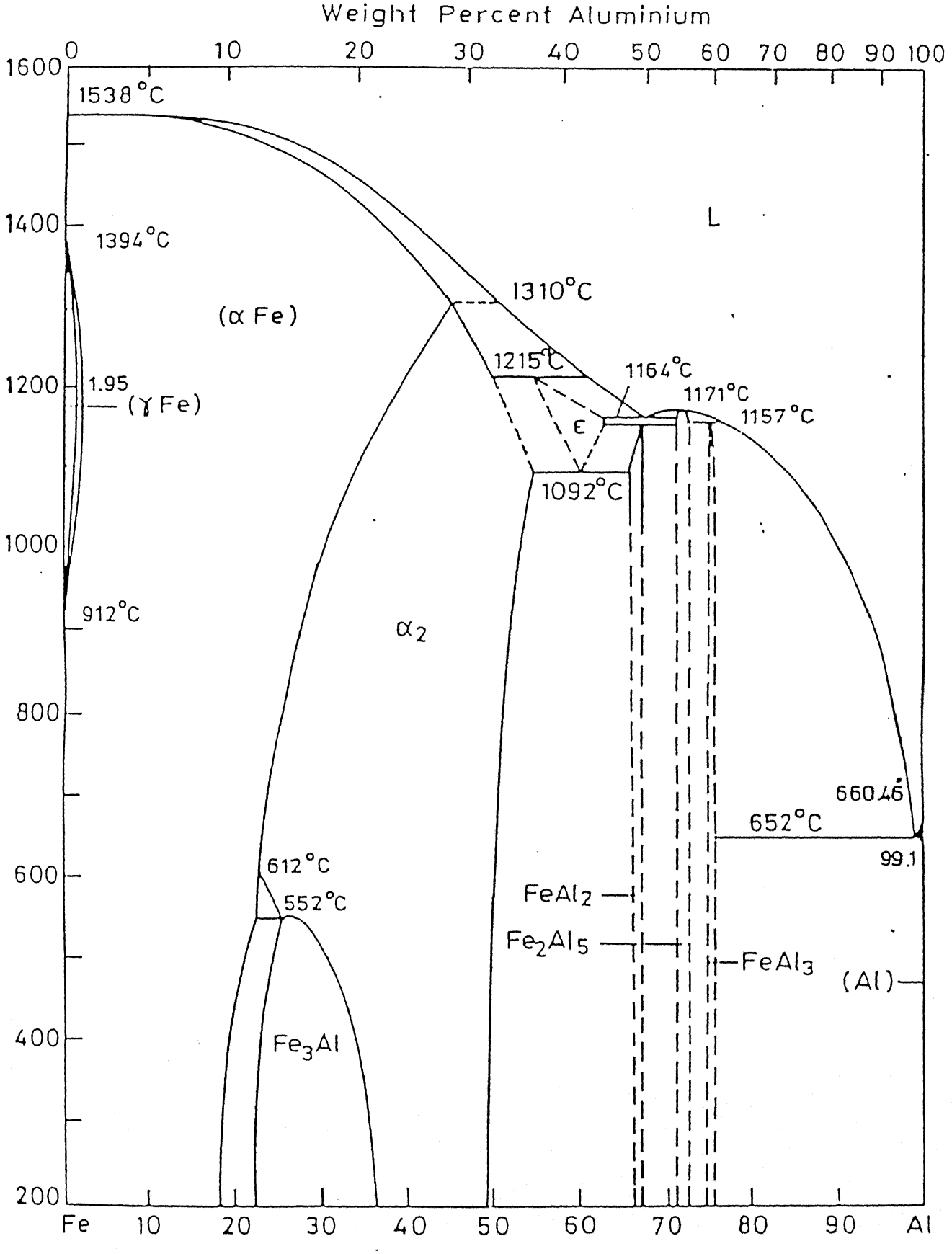
Weight Percent Aluminium
0
10
20
30
40
50
60
70
80
90
100
1600
1400
1200
1000
800
600
400
200
Fe
Al
1538 °C
1394°C
1.95
(γ Fe)
(α Fe)
1310°C
1215°C
1164°C
1171°C
1157 °C
ε
1092°C
L
912°C
α2
612°C
552°C
Fe3Al
FeAl2
Fe2Al5
FeAl3
(Al)
652°C
99.1

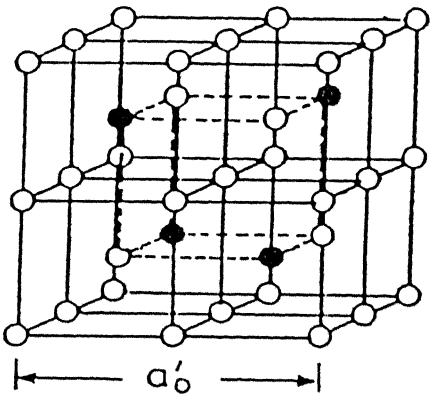

(a) DO_3 unit cell

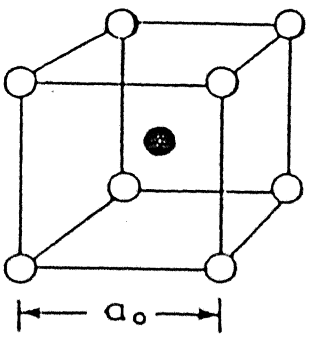

(b) B2 unit cell

Figure 1.2: Ordered Crystal Structure in Fe-Al System.

concentration of quenched in vacancies, with their concentration being approximately twice as high on Fe sites as on Al sites.

In B2-FeAl[8], dislocation configuration consists of two like a<111>/2 dislocations connected by the corresponding a<111>/2 Antiphase Boundary (APB), 'a' being the lattice parameter of the B2 unit cell. The DO_3 dislocation configuration consists of four like a'<111>/2 dislocations connected by two types of APB: (1) the outer pairs of dislocations are connected by an a <111>/2 (a'<111>/4) APB which is affected mainly by first nearest neighbour interaction energies and a similar to a B2 APB, and (2) the inner pair of dislocations are connected by an a'<100>/2 APB which is affected by second nearest neighbour interaction energies. Here, a' is the lattice parameter of DO_3 unit cell.

These configurations are shown schematically in Fig.1.3. Such a configuration is required to preserve both first and second nearest neighbour order in the DO_3 structure during deformation. Formation of the DO_3 structure may be suppressed by quenching alloys from temperatures above Do_3 ordering temperature (Tc). In such cases, the alloys have an imperfect B2 structure and may exhibit B2 dislocation configuration. For an Fe_3Al alloy exhibiting DO_3 and/or B2 order, the APB energy associated with the superlattice dislocations is very low resulting in large extension of the individual dislocation and allowing imperfect configurations. (Fig.1.3(c) and 1.3(d)) to exist. Dislocations travel in Fe_3Al as unit dislocations, leaving ribbons of APB behind on their slip planes. In addition, a preponderance of screw dislocations are observed which in turn give rise to wavy

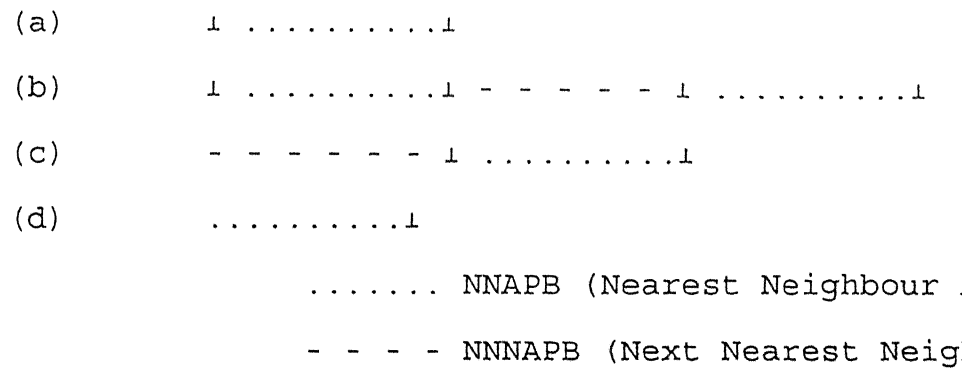

Fig.1.3

Dislocation Configurations in Ordered Fe-Al Alloys

(a) B2 dislocation configuration

(b) DO_3 dislocation configuration

(c) passage of imperfect dislocation in DO_3 lattice

(d) passage of unit dislocation in B2 and DO_3 lattice

slip. The observed preponderance of screw dislocations was attributed[8] to the elastic anisotropy of these materials. It was also found that at compositions of DO_3 ordered alloys containing more than 30at%Al only two a<111>/2 dislocations moved together.These imperfect dislocations generate a'<100>/2 APBs across the slip plane. The transition from perfect (four-fold: Fig.1.3(b))to imperfect (two fold: Fig.1.3(c)) configuration was explained by Crawford et al[8]. They reported B2 and DO_3 APB energies estimated from observation of dislocation separation in superlattice configurations of Fig.1.3(a) and 1.3(b) for Fe-Al alloys containing 26 to 30 at % Al. Their results show that the a<111>/2 (a'<111>/4) APB energy increases whereas the a'<100>/2 DO_3 APB energy decreases with increasing Al content. Therefore, with increasing Al content, the inner separation of the four-fold dislocations (Fig.1.3(b)) increases because of decreasing a'<100>/2 DO_3 APB energy. Therefore, there is an increasing tendency for the outer pair of dislocations to uncouple when the separation is in the range of 0.05 to 0.1 μm.

1.2.3 Properties of Ordered Fe-Al Alloys

1.2.3.1 *Crystallography of Slip & Twinning:*

Slip systems in B2 Fe-Al alloys at 298 K have been reported to be {110} <111>[8]. Slip in FeAl single crystal is a strong function of orientation and deformation temperature. At about 0.44 Tm there is a gradual transition from <111> to <001> slip with increasing temperature. The dislocation arrangement in crystals deformed by <001> type slip consists mostly of edge dislocations. There is also a composition dependence of the slip mode. The slip system in DO_3 alloys is {110} <111>.

Cohn and Coll[8] have shown that in a DO_3 Fe-23.5% Al alloy, mechanical twinning occurred when the degree of long range order was 0.5 or less. Twinning is more easily accomplished in the B2 than in the DO_3 modification of Fe_3Al.

1.2.3.2 *Strength*

The hardness (H)[8] of B2 Fe-Al alloys varies with temperature according to the relation $H = Ae^{-BT}$ where A and B have one set of values at low temperatures and another set at high temperatures. At low temperatures, the hardness increases with increasing Al content while at temperatures greater than 873 K, this behaviour is reversed.

The effect of aluminium content on the yield strength and ductility in 24 at % to 30 at % Al was studied by Mckamey et al[9] (Fig. 1.4). There is a gradual drop in yield strength (from 800 to 300 MPa) accompanied by a steady increase in ductility (from 1 to 5% tensile elongation) with increasing at content in DO_3 Fe-Al alloys. The drop in strength is attributed to a change in deformation mode from the dislocation configuration in Fig. 3(d) to that in Fig. 3(c) because of the increase in nearest neighbour APB energy with increase in Al content. Also, the transition from high stress value from 26 at % Al to a lower value at 27 at % Al coincides with the boundary between the α+DO_3 and DO_3 phase fields at 800°C in the Fe-Al phase diagram (Fig.1.1). Based on this, Inoye[10] has shown that the higher ambient strengths at 24-25 at%Al composition is due to age hardening effect of α-precipitated in DO_3 phase during the ordering treatment at 800°C in these compositions. The ductility increase from 1 % at 24 at % Al to 5% at 30at Al is apparently associated with the drop in yield

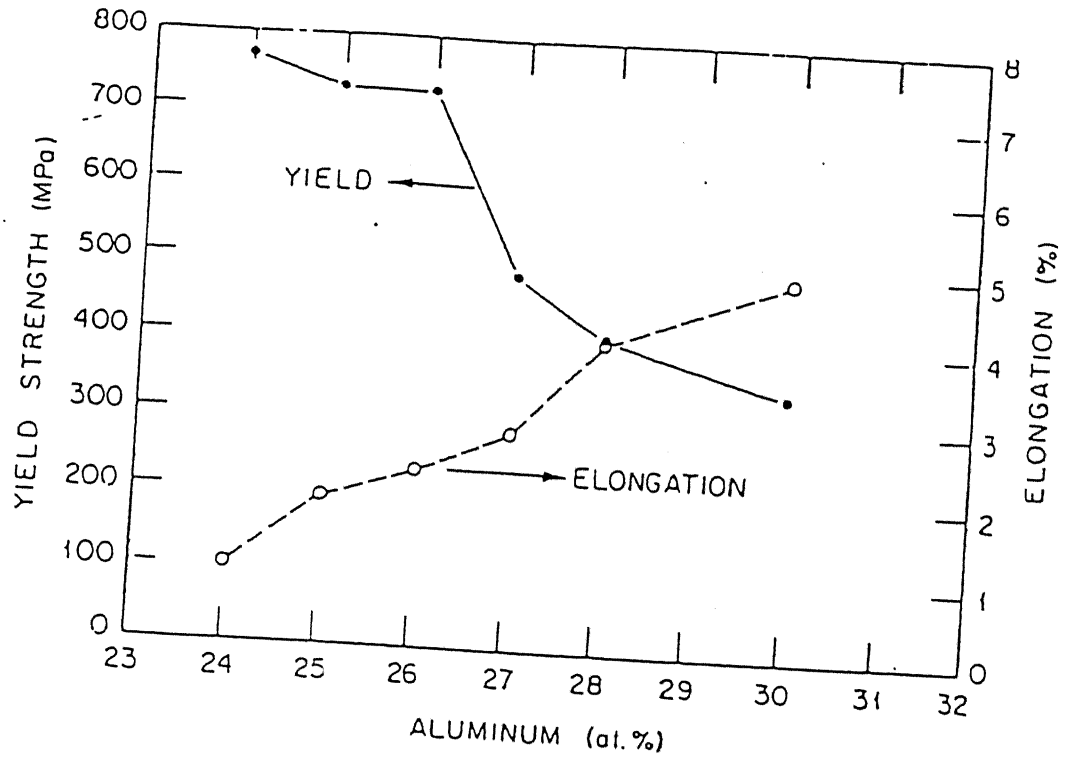

Figure 1.4: Ambient Yield Strength vs. Composition of Fe_3Al.

strength resulting from increasing Al content.

The effect of temperature on the yield strength for the Fe_3Al composition range is shown in Fig.1.5. Here the behaviour of various compositions can be grouped into two regions, one group upto 24 at % Al and another group from 28-30 at % Al composition range. As explained earlier, the higher ambient strength of 24at%Al composition is attributed to the presence of α-precipitates in DO_3 matrix producing age-hardening effect. The second group (28-30 at % Al) exhibit maximum strength peak at approximately 550^oC which corresponds to the second-order transformation temperature from DO_3 to B2. This type of yield behaviour has been observed in many other ordered systems including Ni_3Al, CuZn, Ni_3Mn and FeCo. Alloying studies to raise the transition temperature have been successful in improving the strength levels upto 800^oC.[11] Fig.1.6 shows a typical compressive yield stress plot with temperature of Fe_3Al alloyed with different amounts of Mo & Ti with their respective transition temperatures. The strength peaks in Fe_3Al alloy may be explained by considering the dislocation structure in these alloys. The spacing between the dislocation pair comprising a superlattice dislocation (Fig.1.3(a)) is inversely proportional to long range order parameter (L). At low value of L, this spacing is large and the energy of the connecting APB is small allowing constituent dislocations to glide independently. This process would leave APB trails creating wrong bonds and hardening the alloy. At high temperatures ($T > Tc$) where $L = 0$, the strengthening is mostly due to short-range order (SRO) and is less marked compared to the strengthening in the presence of long range order (LRO). At low

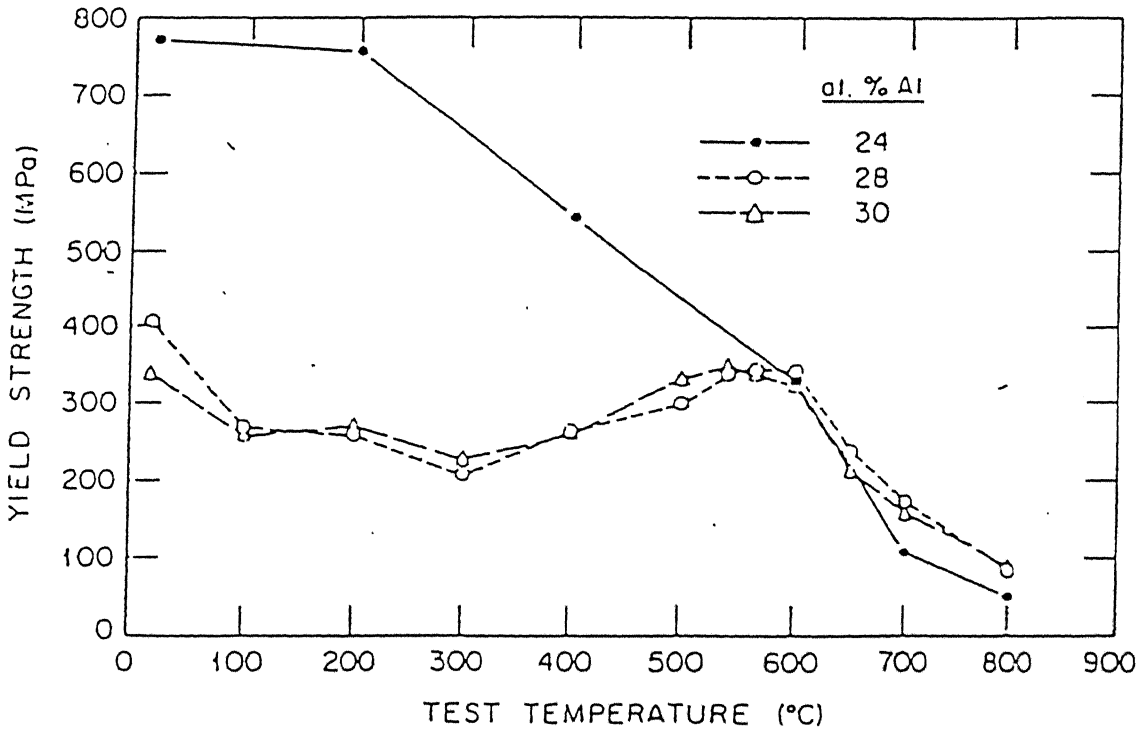

Figure 1.5: Yield Strength vs. Test Temperature for Unalloy
Fe_3Al.

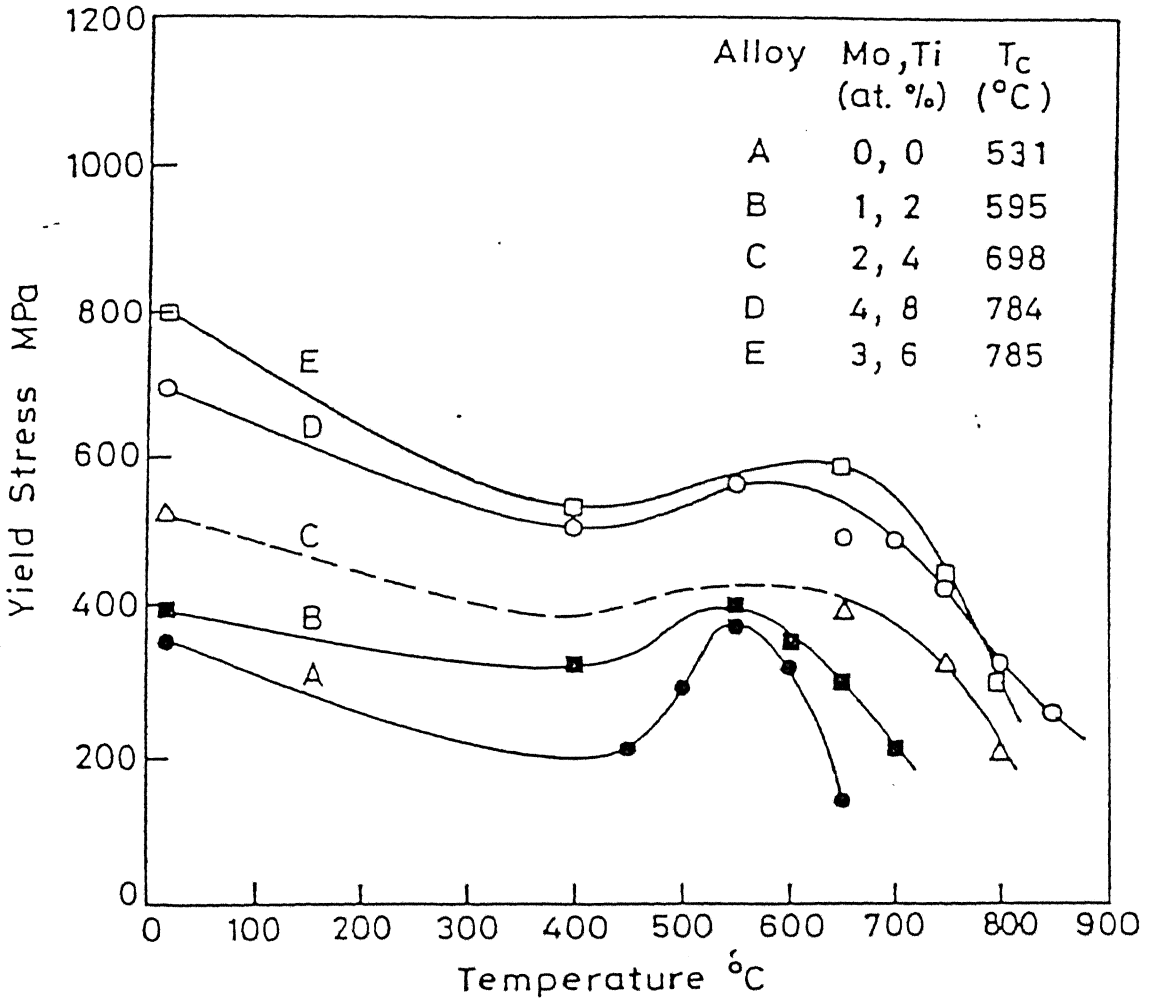

Figure 1.6: Yield Stress vs. Temperature Curves for Alloyed Fe_3Al Shown With Respective Alloy Contents and $DO_3 \longrightarrow B2$ Transition Temperature (T_c).

temperatures, the value of L is large and the unit dislocations tend to associate in pairs. Their motion does not create extra APB's and hence the strength falls as the proportion of superlattice dislocations increases. The strength is a maximum at intermediate values of L where the superlattice dislocation configuration can dissociate into constituent dislocations and corresponds to a spacing of 0.05 to 0.1 μm. In Fe_3Al alloys, this critical degree of long range order parameter (L) related to the peak strength lies in the range 0.5 - 0.6 irrespective of the DO_3 to B2 transition temperature. Also, the value of L is shown to be 0.8 at room temperature.

1.2.3.3 *Work Hardening*

As the degree of DO_3 order increases in Fe_3Al alloy, work hardening also increases. The work hardening behaviour actually observed depends on the deformation temperature (which affects the nucleation of dislocations), the degree of order of the material and its composition which determine the APB energies and hence the shear stresses required to produce them.

1.2.3.4 *Ductility*

As shown in Fig.1.4, there is an increase in ductility with increasing Al content in DO_3 Fe-Al(24at% to 30at%Al) alloys. Room temperature ductility of polycrystalline Fe-Al alloys decreases rapidly with the onset of ordering. For Fe-Al alloy containing more than 30at%Al, the ductility shows a general trend of decreasing with increasing Al level[3] at temperatures upto 400^{o}C. At higher temperatures, the alloys exhibit a peak ductility around 35-38%Al. FeAl is brittle at higher Al contents because it fractures at grain boundaries before yielding. Lower

Al contents reduce the yield stress substantially and hence some ductility is observed before fracture.

A number of workers have reported on the elevated temperature ductility of ordered Fe-Al alloys. 100% elongations were obtained in creep tests on DO_3 Fe-27.8% Al alloys at 826 K. Elongations of 12-16 % were reported for B2 Fe-Al alloys containing 39-49% Al in compression tests conducted at 1300 K.[12]

1.2.3.5 *Fracture*

As stated earlier, iron aluminides are inherently brittle at room temperature. The iron aluminides show low tensile elongations at room temperature and fracture mainly by cleavage for alloys with less than 40at%Al and by brittle grain-boundary separation for alloys with more than 40at%Al[3]. Proposed modes of fracture of Fe-Al alloys are summarised in Table 1.3[8].

The major cause of low ductility and brittle fracture of iron aluminides is mainly by an extrinsic effect-environmental embrittlement.[3] The yield strength is insensitive to environment, and the ultimate tensile strength correlates with the tensile elongation, which depends strongly on test environment. The iron-aluminide (Fe-36.5at%Al) had ductilities of 2% in air, 6% in vacuum and 17.6% in dry oxygen. The lowest ductility was observed in samples tested in water-vapour and the samples tested in molecular hydrogen did not cause severe embrittlement of iron aluminide, so this test indicates that moisture in air is the embrittling agent.

Environmental embrittlement has been explained by the following reaction:

$$2Al + 3H_2O \longrightarrow Al_2O_3 + 6H^+ + 6e^-$$

Table 1.3

Modes of Fracture in Ordered Fe-Al Alloys.

1.	Cleavage on {100} planes by < 100 > edge dislocations.
2.	Cleavage failure due to hydrogen embrittlement.
3.	(a) Cleavage failure due to dislocation APB interactions.
	(b) Intergranular failure in absence of these interactions.
4.	Intergranular failure due to dendritic structure.
5.	Failure at grain boundaries before yielding in bulk.
6.	Intergranular failure due to weak grain boundaries.

The reaction of moisture in air with aluminium atoms at crack tips results in the generation of high-fugacity atomic hydrogen that rapidly penetrates into the crack tips and causes severe embrittlement. The highest ductility is generally obtained in a dry oxygen environment (rather than in vacuum) because oxygen reacts with the aluminium to form aluminium oxide directly, thereby suppressing the aluminium-moisture reaction and the generation of atomic hydrogen. It should be noted that the maximum degree of moisture induced hydrogen embrittlement occurs around ambient temperatures. At higher temperatures, less hydrogen is concentrated at crack tips, and in-situ protective oxide films can form more readily on specimen surfaces; whereas at lower temperatures, the aluminium moisture reaction is slowed, and the equilibrium moisture content in air also is lowered.

The environmental sensitivity of FeAl is markedly reduced when the aluminium concentration is higher than 38 at %. For Fe-43 at % Al, the ductility is almost nil in air as well as in dry oxygen; all specimens fail intergranularly. the lack of an environmental effect is explained by the fact that the grain boundaries in FeAl alloys with Al > 38at% are intrinsically brittle. Therefore, environmental embrittlement and intrinsic grain-boundary brittleness must both be recognised in order to establish strategies for reducing overall brittleness in FeAl alloys. The intrinsic grain boundary brittleness in FeAl as well as other intermetallics, can be alleviated by microalloying with boron, which tends to segregate to the boundaries and enhance their cohesive strength.

Similar air embrittlement has been observed in Fe_3Al alloys. The moisture induced hydrogen affects not only tensile properties, but also the fatigue and crack growth behaviours. Under cyclic loading conditions, vacuum or oxygen environments raise the fatigue threshold and reduce crack growth rates at ambient temperatures. The degree of embrittlement under cyclic loading conditions is also affected by the crystal structure of Fe_3Al. The DO_3 structure in an Fe_3Al alloy shows a crack growth rate much faster than that in the B2 structure, indicating that the DO_3 structure is more susceptible to environmental embrittlement in air.

1.2.3.6 *Creep and Fatique*

The creep resistance of ordered intermetallics may be expected to be better than that of disordered alloys because of slower diffusion in the ordered lattice as well as because of more difficult glide processes.[13,14]

The creep resistance of the binary Fe_3Al alloy is relatively mediocre, but additions of small quantities of Mo and particularly Nb lead to considerable improvements in creep rate and life.[15] These improvements have been attributed to improved solution hardening (for Mo) which reduces the rate of dislocation recovery, as well as to (for Nb) particle dispersion strengthening.

The stress exponent required for creep was found to be approximately 6 which remained constant over the ranges of Al-content (24 to 28at%), temperature (843 to 943 K) and stress (15 to 278 MPa) studied. In contrast, the activation energy for creep was sensitive to Al-content. The creep rate was found to drop suddenly with the onset of DO_3 ordering. The creep rate was

also found to be dependent on grain size, more for a coarse grain size than for a finer grain size for Fe_3Al alloys.[8]

For B2 Fe-Al alloys of Al content 41 to 49%, Whittenberger[12] investigated creep phenomena in the temperature range of 1100 to 1400 K and established that:

(a) The activation energy for creep in these alloys was independent of composition.

(b) Deformation may occur by two different and apparently concentration independent mechanism: one with a stress component of about 6 and the other with an exponent of about 3.

(c) Both the deformation mechanisms are dependent on grain size but in opposite manner. For the low stress exponent mechanism the strength increased with increasing grain size and vice-versa.

(d) Under the high stress exponent mechanism a large-angle grain boundary structure may be replaced by a small-angle structure of similar grain diameter.

The study of high cycle fatigue behaviour of DO_3 and B2 polycrystalline Fe_3Al (Fe-23.7at%Al and Fe-28.7at%Al) reveals that DO_3 order is effective in prolonging fatigue life only in Fe-28.7%at%Al at 298 K. This can be explained by the presence of superlattice dislocations which are not observed in Fe-23.7at%Al. This has been attributed to restrictions on cross slip imposed on superlattice dislocations which delay crack initiation. The fatigue properties of B2 alloys found to degrade sharply with increase in temperature. Among DO_3 alloys, Fe-23.7%Al shows little loss in fatigue life with increase in temperature which is

attributable to its two phase microstructure while Fe-28.7%Al shows a sharp drop with increase in temperature over a range of 293 to 773 K.[16] At temperatures above the two phase field, the fatigue life falls sharply as a result of creep-fatigue interaction. Here, crack initiation occurs at grain boundary near specimen surfaces . but propagation is predominantly by transgranular cleavage.

1.2.3.7 *Weldability & Corrosion Resistance*

Fe_3Al alloys are weldable with careful control of welding parameters and minor alloy additions[1]. Additions of TiB_2 promote hot cracking and are detrimental to the weldability of Fe_3Al alloys. Additions of boron alone also considered to be harmful that produces hot cracking and reduces the weldability. Carbon, on the other hand, appears to be beneficial. Sound weldments have been achieved in Fe_3Al and FeAl alloys using both gas-tungsten-arc welding and electron-beam welding processes. Weld cracking produced by environmental embrittlement is alleviated by pre- and post-weld heat treatments.

The iron aluminides are highly resistance to oxidation and sulfidation at elevated temperature. As stated earlier, resistance stems from the ability of the aluminides to form highly protective Al_2O_3 scales. The oxidation resistance generally increases with increasing Al content, the major products are α-Al_2O_3 and trace amounts of iron oxides when the aluminides are oxidised at temperatures above 900^{o}C. Cyclic oxidation of Fe-40at%Al alloyed with upto 1 at % Hf, Zr, and B, produced little degradation at temperatures upto 1000^{o}C. Aluminides specimen tested at 700 to 870^{o}C showed no indication of attack in

sulfidising environments, except for the formation of a thin layer of oxides with a thickness in an interference colour change. Further, iron aluminides exhibit corrosion rates lower than those of the best existing iron-base alloys by a couple of orders of magnitude when tested in a severe sulfidizing environment at 800°C. In addition, the aluminides with more than 30at%Al are very resistant to corrosion in molten nitrate salt environments at 650°C.

1.2.4 Ternary Additions to Iron Aluminides

Lack of ductility at ambient temperature and a decrease in strength at elevated temperatures have been major obstacle to acceptance of iron aluminides for various structural applications. Considerable effort has been devoted to improve their mechanical properties by means of alloying process and thermomechanical treatments.

Cr additions[8] to Fe_3Al have been reported to lower the yield strength but the ultimate tensile strength of Cr-modified alloy were higher due to work hardening. The room temperature elongation was raised from 4% in Fe-28%Al to 8.2 to 9.4% in alloys with 2-6%Cr. This was accompanied by a change in fracture mode from cleavage to a mixed intergranular-cleavage failure suggesting that Cr enhances cleavage strength. Also, the Fe-Al-Cr alloys showed fine, wary slip lines as opposed to coarse, straight lines in the binary alloy indicating easier cross slip as a result of the Cr-addition. Such ductility enhancement has been related to the improvement in resistance to environmental embrittlement.

The high temperature strength of the Fe_3Al intermetallic is determined largely by the stability of the DO_3 structure relative

to the B2 structures. It is therefore, necessary to increase the $DO_3 \longrightarrow B2 \longrightarrow \alpha$ transition temperatures to strengthen Fe_3Al at elevated temperature. It has been shown that chromium, nickel and molybdenum additions increase these transition temperatures moderately, while silicon and titanium additions in Fe_3Al increase the transition temperature as well as the elevated temperature strength significantly. However, titanium and silicon reduce the room temperature ductility so severely that they have not been considered for further developments. The combined effect of Ti and Mo additions on DO_3 to B2 transition temperature for Fe_3Al alloy is shown in Fig.1.6. The addition of Nb, Cu, Ta, Mn have also been found to raise the transition temperature.[13,15]

Boron, beryllium, zirconium, hafnium have also been found to obtain satisfactory high temperature creep properties and improved ambient temperature ductilities in Fe_3Al. Many of these additions can introduce fine precipitates or dispersoids that reduce grain boundary sliding and inhibit the $DO_3 \longrightarrow B2 \longrightarrow \alpha$ transformation.

In addition to increase the hardness and tensile strength and to improve the ductility of the Fe_3Al intermetallic, nickel[17] addition is found to decrease the size and number of pores in Fe_3Al intermetallic made from powder mixtures. Nickel refines the overall grain size and produces a mixture of fine and coarse grains. In the presence of Ni, fracture of Fe_3Al is mixed transgranular and quasi cleavage.

Small amount of cerium[18] addition has been reported in improving ductility as well as strength at ambient temperature. The improvements of tensile properties and creep-resistance at high temperature can also be achieved by combined addition of

cerium with molybdenum, zirconium or niobium. Cerium addition changes the fracture mode of Fe_3Al based alloys from transgranular cleavage or mixed transgranular cleavage and intergranular fracture to one of transgranular cleavage with portions of dimple fracture.

Small amount of niobium[15] addition to Fe_3Al based alloy has been found to increase the yield strength and creep resistance greatly, but is not beneficial to room temperature ductility. Results of microanalysis indicate that the addition of niobium causes the formation of a lot of precipitates with complex compositions which strengthen both matrix and grain boundaries.

The addition of carbon to Fe_3Al based alloys has been reported to decrease the ductility of these alloys.[19] When carbon content was reduced from 800 to 80 ppm and carbide precipitates were eliminated, the elongation values were found to increase significantly.

1.3 PROCESSING ROUTES FOR IRON ALUMINIDES

1.3.1 Ingot Metallurgy Route

Ingot metallurgy route[20] has been the focus of attention for the production of Ti_3Al, Ni_3Al and Fe_3Al based aluminides for a long period, despite the fact that this route has many problems. The primary fabrication process using the traditional methods of melting and casting poses serious problems, like the alloy inhomogeneity, the elemental loses, the casting defects, fracturing, etc. The secondary fabrication to obtain necessary shapes and sizes by further deformation and machining, poses still further problems as the aluminides are generally brittle in nature.

1.3.1.1 *Melting*

Air melting is feasible for iron aluminide alloys. Reasonable, but not exceptional, care is needed in treating the melt charge and the selection of crucible material. Both the iron and aluminium need to be dried to minimise the generation of hydrogen. Because of the reaction of aluminium with moisture, a large amount of hydrogen can be generated and dissolved in molten metal. It is the rejection of this hydrogen during solidification that causes the gas porosity in iron aluminides. Typical hydrogen levels in the Fe_3Al alloy melted in air can be in the range of 3 to 4 ppm. The hydrogen level of the alloy can be further reduced to approximately 2 ppm by blowing argon through the melt. Vacuum melting of the alloy can yield hydrogen levels of approximately 1 ppm. The protective aluminium oxide slag formation during melting yields low levels of oxygen and nitrogen in the melt and also provides nearly 100% recovery of most of the alloying elements. A combination of vacuum melting and electroslag remelting processes further reduce the oxygen and nitrogen contents of the Fe_3Al based alloys.

1.3.1.2 *Casting*

The Fe_3Al based alloys are castable into shapes by both sand and investment casting processes. The casting parameters such as type of sand, melt superheat, cooling rates, and post-cast treatments are not fully developed for sand castings. In case of investment castings, issues such as shell material, use of grain refiner, shell temperature, melt superheat, cooling rates, and post - cast treatments need additional work. The low room temperature ductility in the as cast condition is the primary

concern in the handling and use of castings.

1.3.1.3 *Mechanical Working*

Fe_3Al based alloys are hot workable with typical hot working temperature ranging between 900 - 1100°C. The hot worked material can be warm finished at temperatures as low as 680°C. The Fe_3Al based alloys are not cold workable.

1.3.2 Powder Metallurgy Route

Powder metallurgy processing is becoming increasingly important for obtaining desirable microstructures, improved properties, and near net shape manufacturing capabilities for iron aluminides. Also, powder metallurgy processes bypass the requirement of melting and casting large ingots and thus greatly reduces the problems associated therein.

There are two types of powder metallurgical processes, one uses prealloyed aluminide powder and the second uses elemental Fe and Al powders as starting materials.

(a) Powder Metallurgical (P/M) processes based on prealloyed aluminide powder

Most powder processing routes for intermetallics utilise rapidly solidified prealloyed powders or ribbons as starting materials, and consolidation is carried out by hot isostatic pressing or hot extrusion[21]. Although successful, these methods involve many processing steps and considerable expenses. High costs may be justified for certain applications by improvements in performance; however, many potential uses for these materials will be realised only if lower cost processing methods emerge.

(b) P/M processes based on elemental powders

This route bypasses the difficulty incurred during the handling of molten metallic solution to produce the prealloyed powders. The process utilises either the elemental or certain master alloy powders which are readily available and inexpensive.

There are two important P/M routes for iron aluminides which use elemental and/or prealloyed powders viz. reactive sintering and mechanical alloying.

1.3.2.1 *Reactive Sintering Route*

Reactive sintering (also known as combustion synthesis, or self - propagating high temperature synthesis) is a novel process to produce ordered intermetallics from elemental powders. Through self - sustaining reaction. This approach utilizes an exothermic reaction between powder constituents to synthesize compounds[22].Process advantages include the use of inexpensive and easily compacted elemental powders, low processing temperatures, short processing times, and considerable flexibility in terms of compositional and microstructural control. Depending upon thermodynamic properties and phase diagram features, a variety of reaction products are possible, ranging from highly porous to fully dense cast materials.

Reactive sintering is controlled by a transient liquid phase that forms during rapid exothermic heating. The initial compact is composed of mixed powders which are heated to a temperature where they react to form a compound product. Fig.1.7shows a schematic binary phase diagram where reaction sintering can be anticipated with various steps associated. Here, a stoichiometric mixture of A and B powders is used to form an intermediate compound product AB.

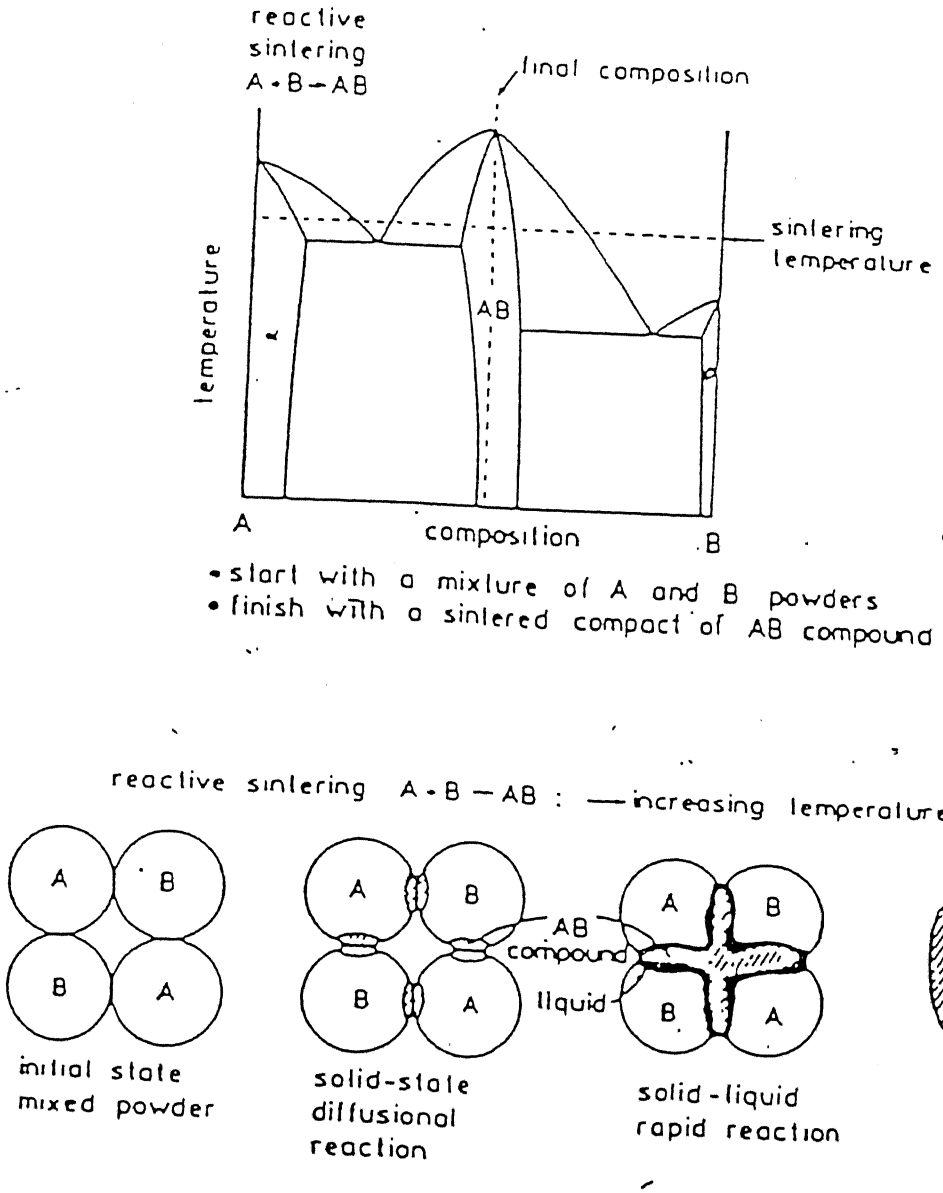

Figure 1.7: A Typical Binary Phase Diagram for a Reactive Sintering System shown with Various Schematic Stages of Compound Formation.

The reaction occurs above the lowest eutectic temperature in the system yet at a temperature where the compound is solid. Heat is liberated because of the thermodynamic stability of the high melting temperature compound. Consequently, reactive sintering is nearly spontaneous once the liquid forms. The liquid provides a capillary force on the structure which leads to densification. The liquid is transient as the process is conducted at a temperature below the melting temperature of the compound, typically near the eutectic.

Reaction sintering involves a transient liquid phase, duration and amount of which depends on several processing parameters and which in turn control the sintering characteristic. The reaction sintering is highly sensitive to parameters such as amount of additive and particle size, green density of initial compact, heating rate, sintering atmosphere and sintering time.

The intent of prior studies on Fe-Al was not to form intermetallic compounds as products; nevertheless, the observations reported emphasise the problems encountered in this system. Elemental iron - aluminium mixture represent a particular challenge for powder processing because extensive compact swelling occurs. Swelling is predicted based upon phase diagram features (Fig.1.1); notably, there is a large solubility for aluminium in iron, low reverse solubility, and a large melting point difference, suggesting imbalanced diffusion rates. Systems that exhibit a large driving force for compound formation are particularly susceptibility to the formation of porosity during alloying. Synthesis of iron aluminide from elemental powders has been reported in the literature. Reaction chemistry in Fe-Al,

studied using differential scanning calorimetry (DSC) is shown in Table 1.4.

The conventional reactive sintering involves no pressure that is, it is a pressureless sintering. The highest sintered densities obtained by Rabin and Wright[22] were approximately 75% of theoretical for Fe-15.8wt%Al and 69% of theoretical for Fe-32wt%Al in pressureless reactive sintering. The higher sintered density can be obtained by applying an external pressure to the compact during sintering. This process is known as hot pressing. Here, pressure assisted densification is carried out by applying a load to the samples during the exothermic reaction. Rabin and Wright also observed the effect of applied pressure on density for both Fe-15.8wt%Al and Fe-32wt%Al compositions which is shown in Fig.1.8. Near full density was achieved for both compositions when an applied pressure of 70 MPa was used. Significantly, higher densities were also obtained for a given applied pressure when the larger powder charge was used. This suggests that the larger thermal mass resulted in slower cooling from the reaction temperature, thus allowing more densification to take place.

1.3.2.2 *Mechanical Alloying Route*

It is quite difficult to alloy by conventional techniques a metal with a high melting point and one with a low melting point. Even though two such metals may form a solution in the liquid state, the metal with the lower melting point tends to separate out in the course of cooling and solidification. Mechanical alloying was developed to overcome this problem around 1966 at International Nickel Company (INCO) by Benjamin and coworkers. Mechanical alloying circumvents many of the limitations of

Table 1.4

Reaction Chemistry Results in Fe-Al.

Atom %	Reaction Temp. (K)	Heating Rate (K/min)	$-\Delta H^{\circ}_{298}$ KJ/g atom	Phase Present
50 Fe-50 Al	911	15K/min	19.6	AlFe, Al_5Fe_2, Fe
75 Fe-25 Al	916-984	15K/min	7.69	Fe_3Al, Fe

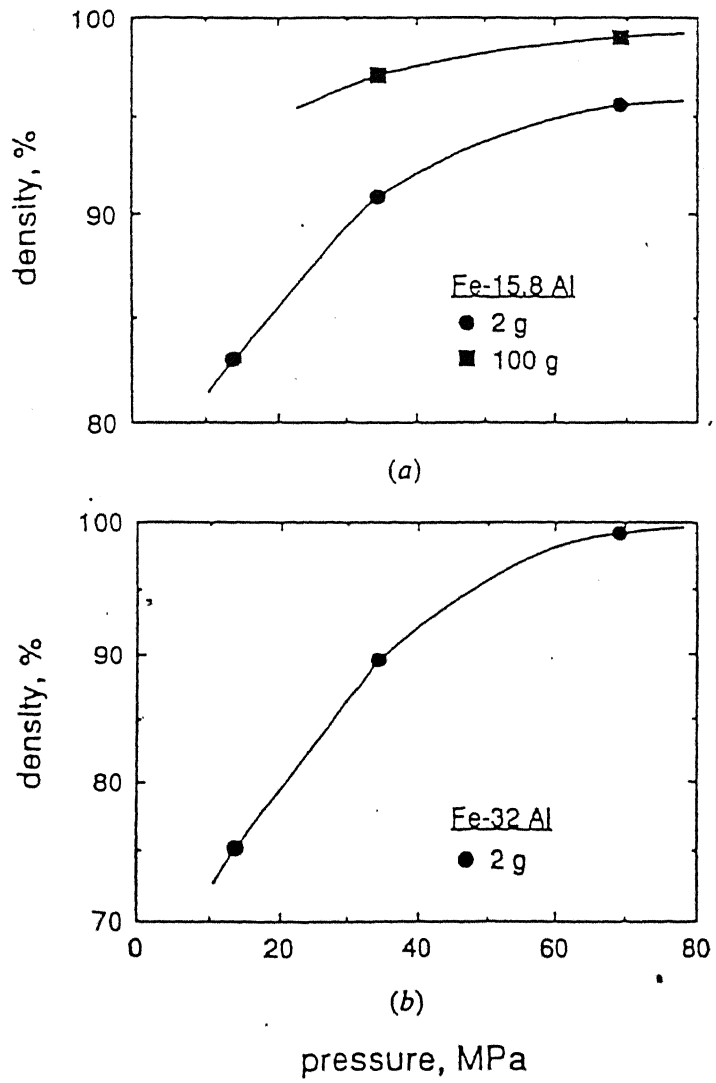

Figure 1.8: Density as a Function of Applied Pressure for Reaction Hot Pressing Powders of
(a) Fe-15.8wt%Al and
(b) Fe-32wt%Al.

conventional alloying. It creates true alloys of metals and metal oxides that are very difficult or impossible to combine by other means.

Mechanical alloying is a dry, high energy milling process[23-25]. It occurs by the repeated welding and fracturing of a mixture of metallic and/or non metallic powders in a highly activated ball charge. The raw materials used in Mechanical Alloying (MA) must include at least one fairly ductile metal to act as a host or binder to hold together the other ingredients. Ductile metals that have been used include nickel, copper, iron, aluminium and even such normally brittle metals as chromium. Under the extreme state of hydrostatic compression that exists when powder particles are trapped between colliding grinding balls, materials that are brittle under tensile loading will undergo fairly large amounts of plastic strain before fracture. Other ingredients can includes brittle intermetallic compounds such as aluminides. Substantial amounts of non metallic ingredients including oxides, carbides, nitrides and elements such as carbon, and boron can be added. Alloying additions can also be made by doping the milling atmosphere.To reduce cold welding and promote fracturing, a suitable Processing Control Agent (PCA) which is generally an organic compound is added. After the milling procedure, the organic additives may be removed by evaporation. Since, the force of impact deforms the particles and creates atomically clean new surfaces and such surfaces readily oxidise, the milling operation is conducted in an atmosphere of nitrogen or an inert gas.

MA process can be described as consisting of several stages[23]

as schematised in Fig.1.9. (It must be understood that MA is statistical in nature, however, thus, each particle experiences a unique processing history). The first stage involves powder mixing and concurrent deformation, fracture and welding of powder particles. The deformation and welding cause the formation of large flake shaped particles and composite particles containing layers of the alloy components. A significant variability is seen in the morphology and hardness of the particles during this stage due to the statistical nature of the process.

In the next stage, the welding of powder particles dominates. Thus, the particle size increases and the number of particles decreases concurrently. Particle hardness continues to increase due to the extensive plastic deformation taking place during MA. The subsequent two stages are those of equiaxed particle formation and welding of layered particles producing "random" particle orientations. During these stages there is a decrease in the fraction of large flake shaped particles and the lamellar structure of the particles not only becomes progressively finer but also manifests a convoluted or marbled structure. The continuing increase in particle hardness and concurrent decrease in ductility lead to an increased tendency for particle fracture.

Steady-state processing constitutes the final MA stage. The composition of each particle converges to the overall composition, and hardness approaches a saturation value. During steady-state processing, there is a reasonable balance between the frequencies of particle fracturing and welding. Thus, the average particle size does not change much during this stage nor does the distribution in particle size.

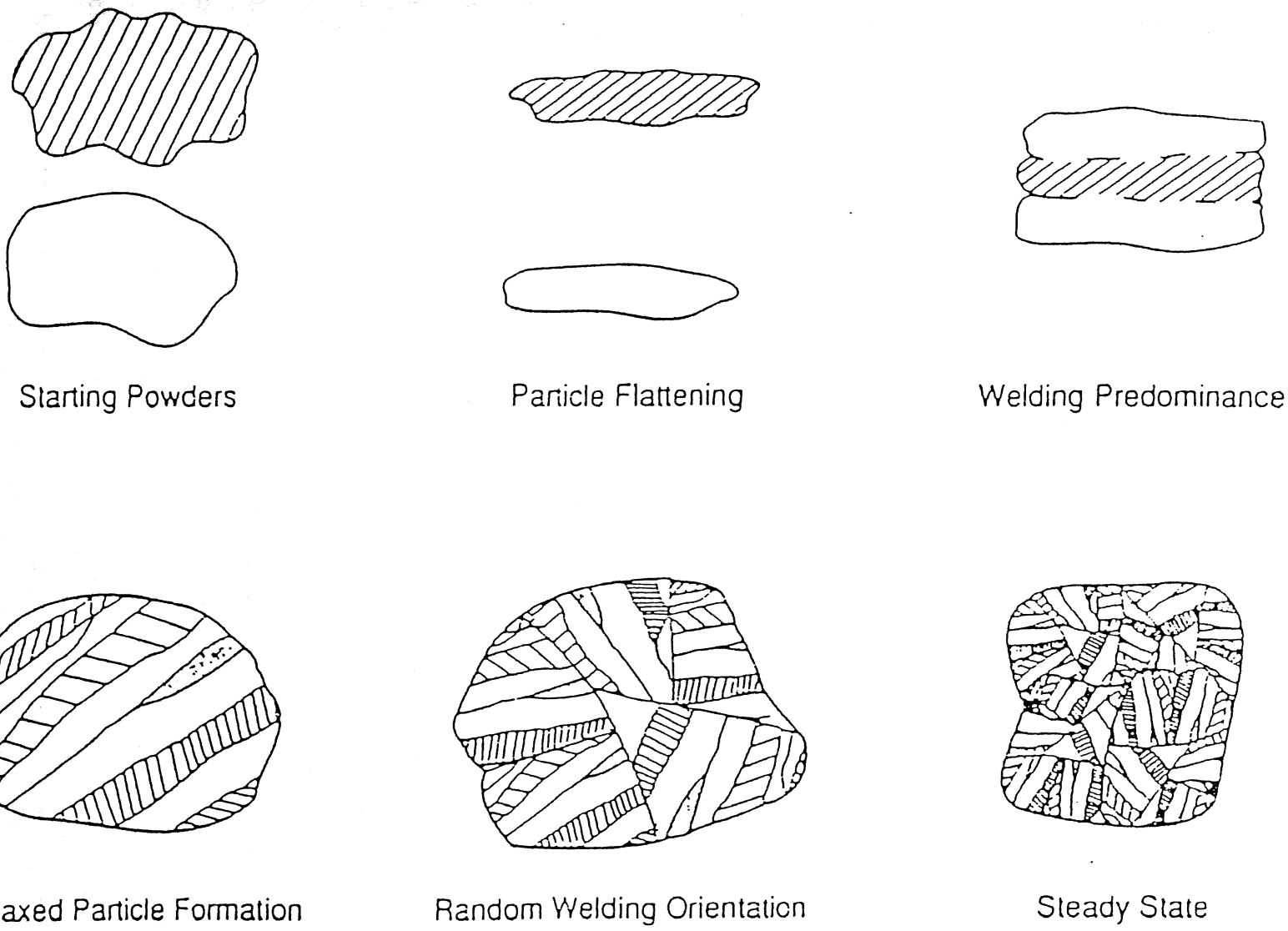

Figure 1.9: The Several Stages that Ductile Metals Undergo During Mechanical Alloying.

The mill, where the MA processing is performed, is usually one of three common configurations as shown in Fig.1.10[25]. One is a vertical ball mill such as the Szegvari attritor (Fig.1.10(a)) which can be used to produce moderate volumes of material in "moderate"milling times (typically, on the order of hours). In this device, the ball and powder charges are held in a stationary vertical tank and are agitated by impellers radiating from a central rotating shaft.

A second configuration is the vibratory mill, exemplified by the SPEX shaker mill (Fig.1.10(b)). Such a machine can produce small quantities of mechanically alloyed powder in relatively short times (typically, in less than an hour). In this system, the ball and powder charges are placed in a small vial which is agitated at a high frequency in a complex cycle which involves motion in three orthogonal directions.

A third type of machine that can be used for MA is a conventional horizontal ball mill (Fig.1.10(c)). In such a mill, the powder and ball (long rods are sometimes used) charges are placed in a large (>1 m in diameter)drum, which is rotated about its central horizontal axis at a speed just below the critical speed that would pin the balls to the internal wall of the drum. Mills of this nature are used to produce large volumes of powder, but processing times are typically long.

Recently, MA technique has been extended to greatly refine the microstructure of the matrix into the nanometer range and to the synthesis of novel phases including supersaturated solid solutions, crystalline and quasi crystalline intermediate phases and metallic glasses produced from either blended elemental or pre

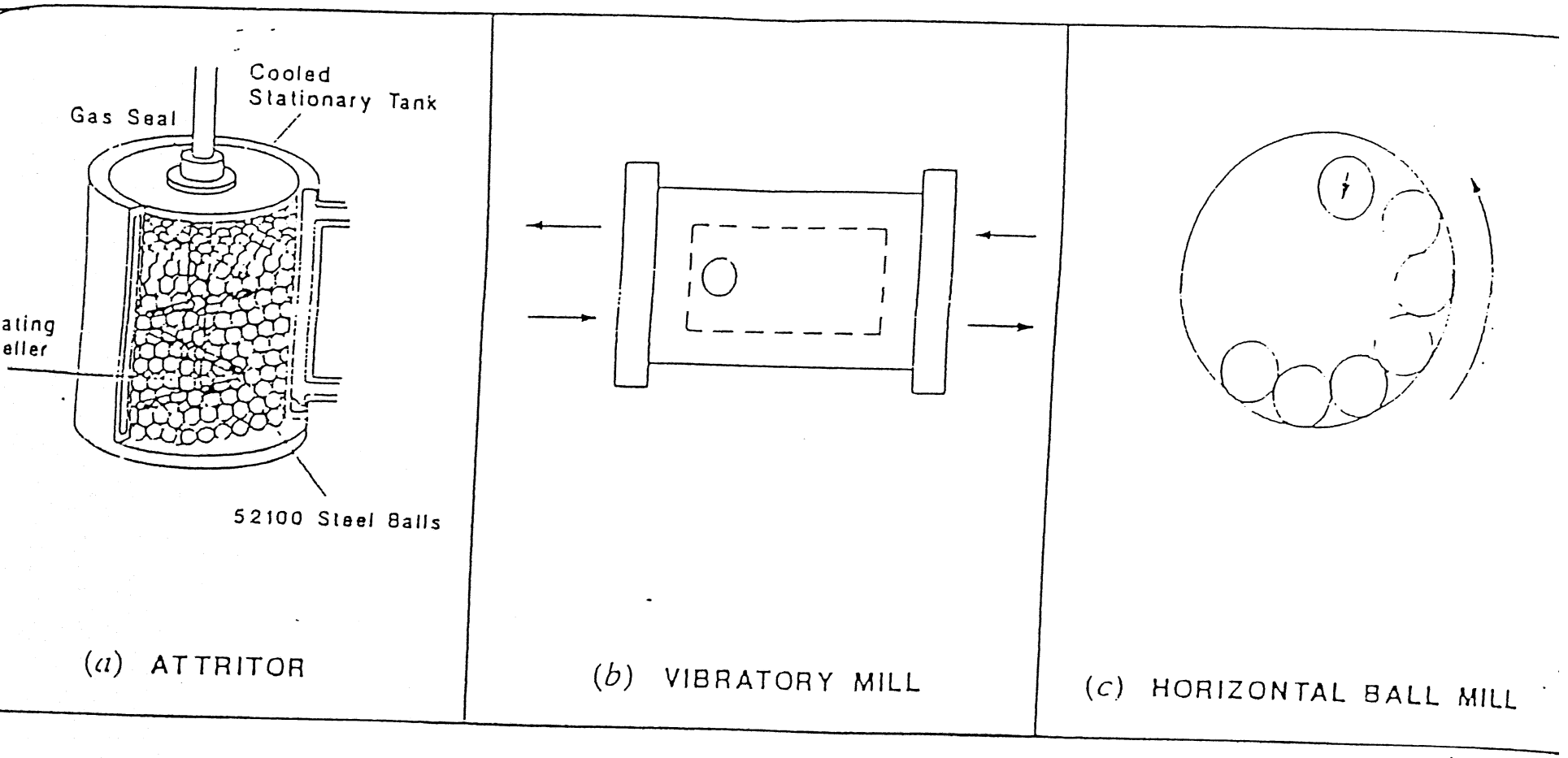

Figure 1.10: Some Common Devices Used for Mechanical Alloying
(a) An Attritor
(b) a SPEX Shaker (or Vibratory) Mill
(c) A Conventional Horizontal Ball Mill

- alloyed powders. Besides these attributes, MA has the advantage of not involving melting, allowing alloying of elements with significantly different melting points, and it is a process scaleable to commercial size[26].

Although several intermetallics are produced by conventional ingot metallurgy techniques, synthesis by MA offers potential advantages. Firstly, since MA is a solid state powder processing technique, complex solidification paths can be bypassed and problems associated with the narrow composition ranges of some intermetallics can be minimised. Secondly, MA is known to produce nanometer grains in all metallic systems and the room temperature creep deformation rate is several order of magnitude higher in nanocrystalline materials; this can lead to enhanced ambient temperature ductility.

Due in part to its simplicity, MA has becomes a general tool used by material scientists to prepare a variety of alloy powders with metastable phases and/or microstructure. It is difficult, however, to predict the product of MA for a given starting powder[27]. In general, the product depends on the milling parameters such as processing time and temperature, milling energy, and type of process control agent used. Another parameter which can strongly influence the MA product, is contamination of the powder product during the processing. Contamination may arise from erosion of the milling media, gas leaked into milling vial, or from the process control agent. Even minute amounts of contamination, hardly detected by energy dispersive x-ray analysis can in some cases change the structure of the product and therefore properties.

Mechanical Alloying in the Fe - Al system:

Mechanical alloying in the other intermetallic systems like Ni-Al, Ti-Al has been reported extensively MA in the Fe-Al system has been the focus of attention for last few years.

Fair and Wood[28] produced Fe_3Al intermetallic from elemental powders by the heat treatment of mechanically alloyed iron and aluminium powders. They found it was a result of a two stage process, a mixture of iron and the intermetallic FeAl being produced during the initial milling stage and the intermetallic Fe_3Al forming by the coalescence of these two phases during subsequent heat treatment. The Fe_3Al produced by this technique had the B2 structure and not the equilibrium DO_3 structure. This is unusual since the actual composition of the compound was that of Fe_3Al (DO_3). Mechanical alloying introduces a very large degree of structural damage and the high number of defects created are responsible for the production of the B2 structure in preference to DO_3 structure. Such an effect has, also, been observed in rapidly solidified Fe_3Al and has been attributed to the presence of quenched in vacancies. Hardness testing of the heat treated material indicated that the intermetallic produced by this technique was ductile and this had been attributed to a very fine grain size and good homogeneity.

Morris et al[29] studied MA in the FeAl phase with an aluminium content of 35 atomic%. Process control agent used was 0.5 wt% carbon which was added as finely divided graphite. Both aluminium carbide, Al_4C_3, and perovskite, $Fe_3AlC_{0.5-0.7}$, were formed as fine dispersoid particles distributed through the alloy. A fine grain size (about 1-2 μm) was obtained. The strength (700 - 900

MPa) was high, but tensile ductility was very low (about 2%) which was believed to be caused by the high interstitial impurity content. An increase in ductility was found by ageing to precipitate out carbides.

Oleszak et al[30] applied MA to alloy synthesis from Fe-Al powder mixtures containing 10, 20, 30, 40 & 50 wt% Al. An evolution of the powder morphology from flaky in the first stage to spherical in the final stage was observed. For all alloys studied, a disordered b.c.c. solid solution was observed by ball milling. A grain size of several nanometers and a maximum r.m.s. strain level upto 1% was observed. The charge in lattice parameter found to be upto 2.4%.

Deane and Cochrane[31] observed the effect of process variables on the MA of iron aluminide (Fe-25at%Al) in a planetary ball mill. A disordered b.c.c. solid solution of Al in Fe was formed. TEM observations showed that the aluminium particles reached temperatures sufficient to allow recrystallisation of aluminium grains during the earlier stages of milling process. They also found that for aluminium starting powder size smaller than that of iron, a fine lamellar structure occurred at a much faster rate due to the increased rate of flow of the aluminium particles around the larger iron particles. The rate of formation of solid solution was found to be faster in powders milled with a large number of small milling media than a small number of large milling media.

1.4 AIMS OF THE PRESENT STUDY

The aims of the present investigation are:

(i) To study the process of mechanical alloying of a mixture of Fe-Al-Cr powders corresponding to Fe-28at%Al-5at%Cr

composition in a high energy mechanical attritor.

(ii) To study the effect of subsequent powder metallurgical processing routes on mechanically alloyed powder. The two powder metallurgical processing routes were employed. The first route involved cold compaction of mechanically alloyed powder and its subsequent sintering and hot rolling. The second route was the hot pressing of mechanically alloyed powder.

CHAPTER 2

EXPERIMENTAL PROCEDURE

2.1 RAW MATERIALS

The starting materials used were elemental iron, aluminium and chromium powders. Electrolytic iron powder (> 99.0% purity) supplied by Sudhakar Products, Bombay and having the following chemical analysis was used:

Fe (min.)	99.00
C	0.025
S	0.02
H2 Loss	0.3
Other Impurities	0.11

The mesh analysis of iron powder is given below:

+ 200	40
+ 325	30
- 325	30

99.9% pure atomised aluminium powder, supplied by Metal Powder company Ltd., Madurai (Tamil Nadu) and 99% pure chromium (Chemical Reagent Grade) powder were used.

The scanning electron micrographs of elemental iron and aluminium powders used are shown in Fig. 2.1.

2.2 MECHANICAL ALLOYING

A mixture of 1 kg. powder was prepared by mixing 786.9 gm of iron powder, 158.60 gm of aluminium powder and 54.50 gm of chromium powder which corresponds to Fe-28at%Al-5at%Cr

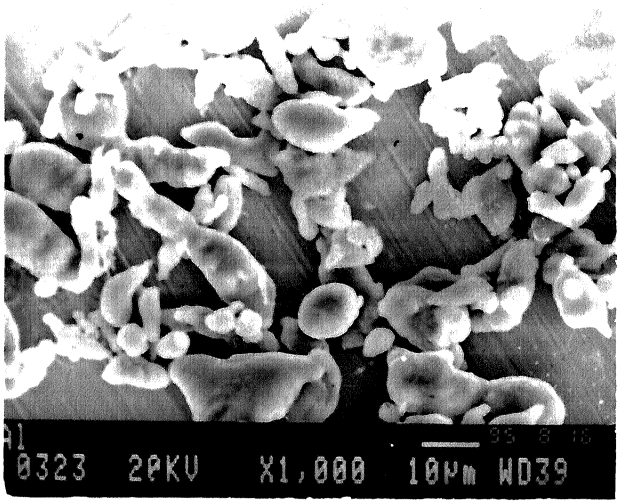

(b)

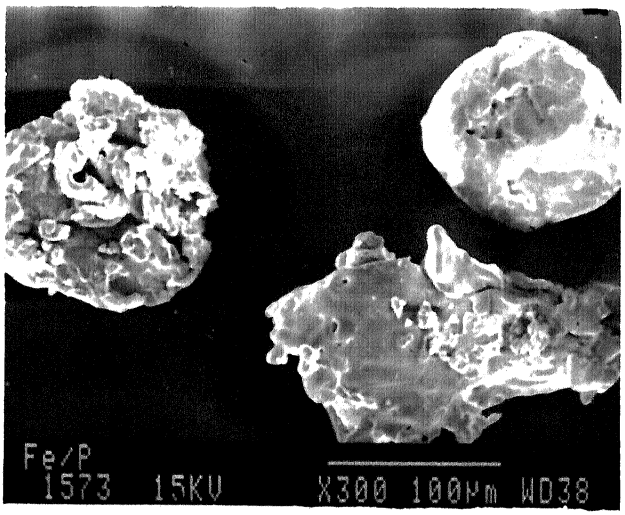

(a)

Figure 2.1: (a) SEM Micrograph of Fe Powder
(b) SEM Micrograph of Al Powder

composition. The premixed powder was milled in a high energy T.C. Attritor Mill (Torrance, U.K.). Tungston carbide balls of diameter 9 mm. were used as grinding media. The ball to powder weight ratio was 12:1. The mill had a water cooling arrangement to minimise the temperature rise of the powder during milling. Process controlling agent (PCA) used was acetone to promote fracturing and to reduce excessive welding of the powder particles during milling. The milling was carried out in air. The milling was carried out at speed of 500 rpm. Small quantities of powders were withdrawn from the mill after different intervals of time (2 hrs, 4 hrs, 8 hrs, 16 hrs, 32 hrs, 40 hrs, 50 hrs, 60 hrs, 70 hrs, and 80 hrs.) to study the progress of mechanical alloying.

2.3 COLD COMPACTION, SINTERING AND ROLLING OF MECHANICALLY ALLOYED POWDER

2.3.1 Cold Compaction of Mechanically Alloyed Powder

Mechanically alloyed powder obtained after 80 hrs of milling was compacted into cylindrical shape in a steel die (diameter - 31 mm) on 50 T hydraulic press under three different compaction pressures of 97 MPa, 195 MPa and 318 MPa. The weight of the powder taken for each compact was approximately 15 gm. Zinc stearate was used as lubricant.

2.3.2 Sintering of Green Compacts

The green compacts so obtained from Section 2.3.1. were sintered in a horizontal tube INCONEL furnace with SiC heating elements. The furnace was closed from one end and had the provision for maintaining a protective atmosphere. The temperature of sintering was 1100^{o}C and the duration of sintering were 30 min and 120 min. The argon gas (I0LAR-1 grade) was used

as sintering atmosphere throughout the experiment.

2.3.3 Hot Rolling of Sintered Compacts

The sintered compacts obtained from Section 2.3.2 were preheated in the INCONEL furnace at 1100°C under argon atmosphere for 30 min. A 2 mm diameter hole was drilled in the sintered compacts before preheating through which a steel thread was tied to enable handling during hot rolling. The hot rolling of the sintered compacts was done by bringing the furnace near to the nip of the rolls of 2 Hi-Mill and pulling the sample out of the furnace with the help of the steel thread.

2.4 HOT PRESSING OF MECHANICALLY ALLOYED POWDER

The powder obtained after 80 hrs. of milling was hot pressed utilising the hot-press of Dr. FRITSCH KG, West Germany. the graphite die of 8 mm diameter was filled with mechanically alloyed powder. It was then loaded with graphite punch, and a constant pressure of 20 MPa was applied during hot pressing. The hot pressing was done at four different temperatures of 800°C, 900°C, 1000°C and 1100°C. The requisite temperatures were obtained by resistance heating of graphite die. The temperature was continuously monitored by a chromel-alumel thermocouple inserted into the graphite die wall. The holding time of 5 - 15 minutes were employed. A schematic sketch depicting hot-pressing set-up is shown in Fig. 2.2. Boron nitride was used as lubricant.

2.5 CHARACTERISATION METHODS OF MECHANICALLY ALLOYED POWDERS, SINTERED AND HOT PRESSED COMPACTS

2.5.1 X-Ray Analysis

Powder samples taken out after different intervals of time were used for X-ray diffraction with Cu-Kα radiation. The 2θ

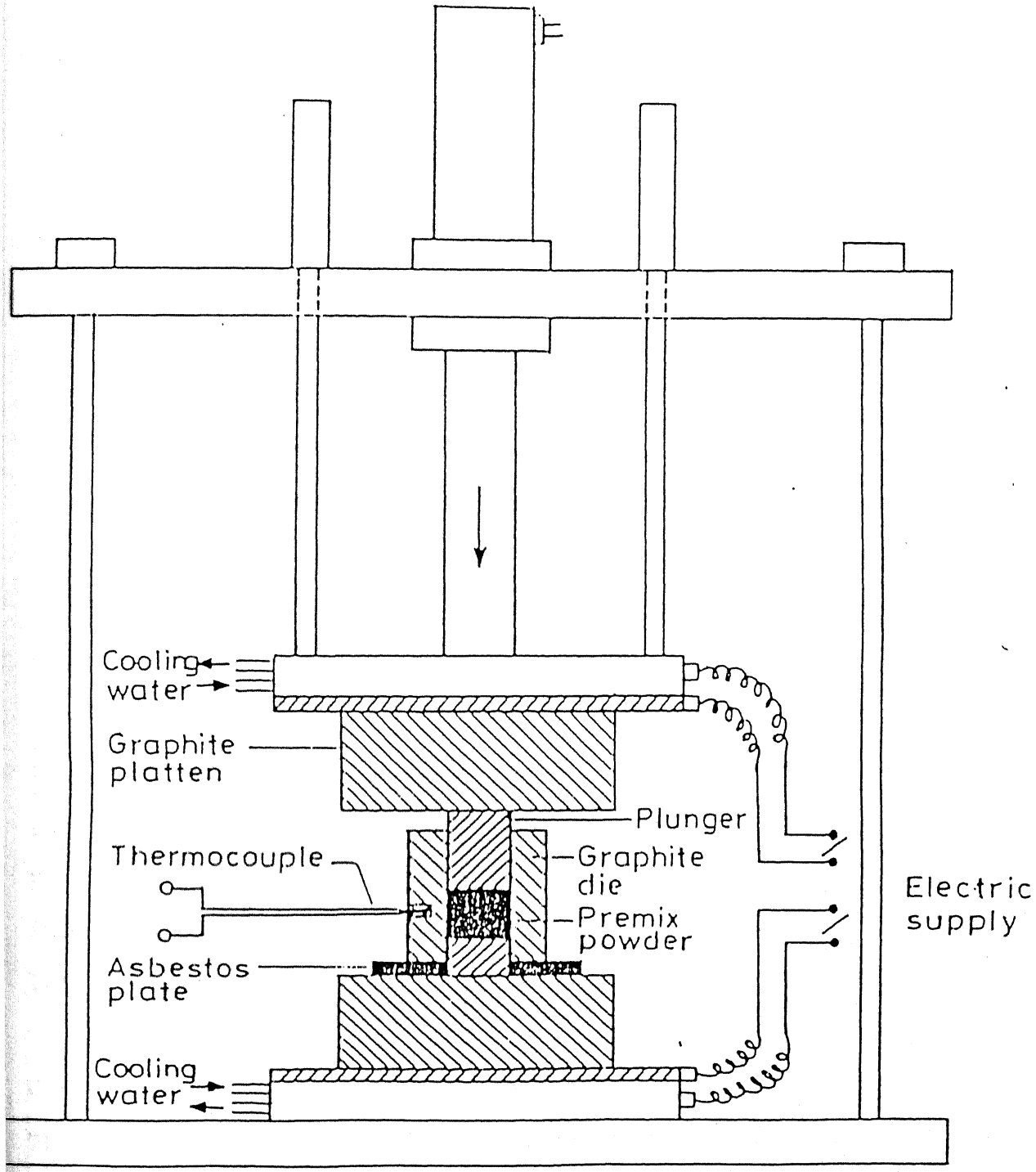

Figure 2.2: A Schematic Sketch of Hot Pressing Set-up.

values were obtained directly through X-ray diffraction. The wavelength of Cu-Kα radiation was taken to be 1.5406 A^{o} and d-values corresponding to each 2θ value were calculated for each powder sample. These d-values were directly compared with standard d-values given in JCPDS Powder Diffraction files to identify the phases. The diffraction patterns were obtained under the following conditions;

Voltage	30 KV
Current	20 mA
Scanning Speed	3^{o} per minute (in 2θ values)
Chart Speed	3 cm per minute
Time Constant	10 Sec.

The conditions were kept constant for all the samples studied.

2.5.2 Scanning Electron Microscopy (SEM)

JEOL JSM 840A Scanning Electron Microscope (with EDAX facility) at an operating voltage of 15 KV was used for observing powder samples, sintered and hot pressed compacts.

The sintered and hot pressed compacts for SEM were prepared by first polishing the samples on belt and then on emery paper of grades 0/1, 0/2, 0/3 and 0/4 followed by fine alumina wheel polishing. The etchant used was 33% CH_3COOH, 33% HNO_3, 33% H_2O and 1% HF.

2.5.3 Density and Porosity Measurements

The densities of sintered compacts were measured by the displacement method. The dried samples first weighed in air (W_A). These were, then, xylene impregnated by putting the sintered compacts dipped in xylene liquid in a vacuum desiccator under a constant suction for 2 hrs. The impregnated samples were first

weighed in air (W_B) and then weighed in fully submerged water (W_C). The sintered densities were measured using the Arthur formula:

$$\text{Sintered density} = \frac{W_A}{W_B - W_C} \text{ gm/cc}$$

$$\text{And \% Porosity} = \left(1 - \frac{\text{Sintered Density}}{\text{Theoretical Density}} \right) \times 100$$

The theoretical density for all sintered and hot pressed compacts was assumed to be 6.69 gm/cc which corresponds to density of Fe_3Al intermetallic.

The densities of the green and hot-pressed compacts were measured by physical measurement.

2.5.4 Hardness Testing

Microhardness measurement were made on all sintered and hot-pressed compacts using a Leitz Miniload Microhardness tester. The various readings were taken to note the variation of microhardness from one region to another.

Rockwell hardness was measured using C scale on a Rockwell Hardness Tester. The five points were taken on each sample for accurate determination of hardness.

2.5.5 Compression Testing

Compression tests were carried out using an INSTRON universal testing machine. On a full scale load of 100 KN. The compressive strength were calculated from the load applied divided by the initial area of the compact.

2.5.6 Electron-Probe Micro-Analysis (EPMA)

To obtain point analysis of compacts, Electron Probe Micro-Analysis (EPMA) technique has been used. In this micro-analysis, a small electric probe (~ 100 nm diameter) is used

to generate x-rays from a defined area of a polished specimen and the intensity of various x-rays measured using wavelength dispersive spectrum spectrometer (WDS).

CHAPTER 3

RESULTS AND DISCUSSION

3.1 MECHANICAL ALLOYING OF Fe-Al-Cr POWDER

The mechanical alloying of a mixture of Fe, Al and Cr powder was done for a period upto 80 hrs. in a high energy mechanical attritor. The effect of milling time on various characteristics were studied by taking out samples from the attritor after different intervals of time. The results obtained are discussed in the following subsections.

3.1.1 Effect of Milling Time on the Progress of Mechanical Alloying

The progress of mechanical alloying with milling time was observed through X-ray diffraction patterns for different powder samples which were taken out after different intervals of time. The X-ray diffraction patterns for some selected time intervals are shown in Fig. 3.1. Standard data for X-ray diffraction of some important elements and compounds are shown in Table 3.1. There is no standard data for X-ray diffraction of solid solution of Al in Fe which is expected to be formed in the present study. The peaks obtained from (200), (220), (222), (400), (420) and (422) planes of elemental Al and peaks obtained from (110), (200), (211), (220), (310), (222) planes of elemental Cr. are very close to peaks obtained from (110), (200), (211), (220), (310), (222) planes of elemental Fe respectively. Therefore, the progress of mechanical alloying was monitored by observing peaks of (111), (311), (331) planes of elemental Al which do not overlap either

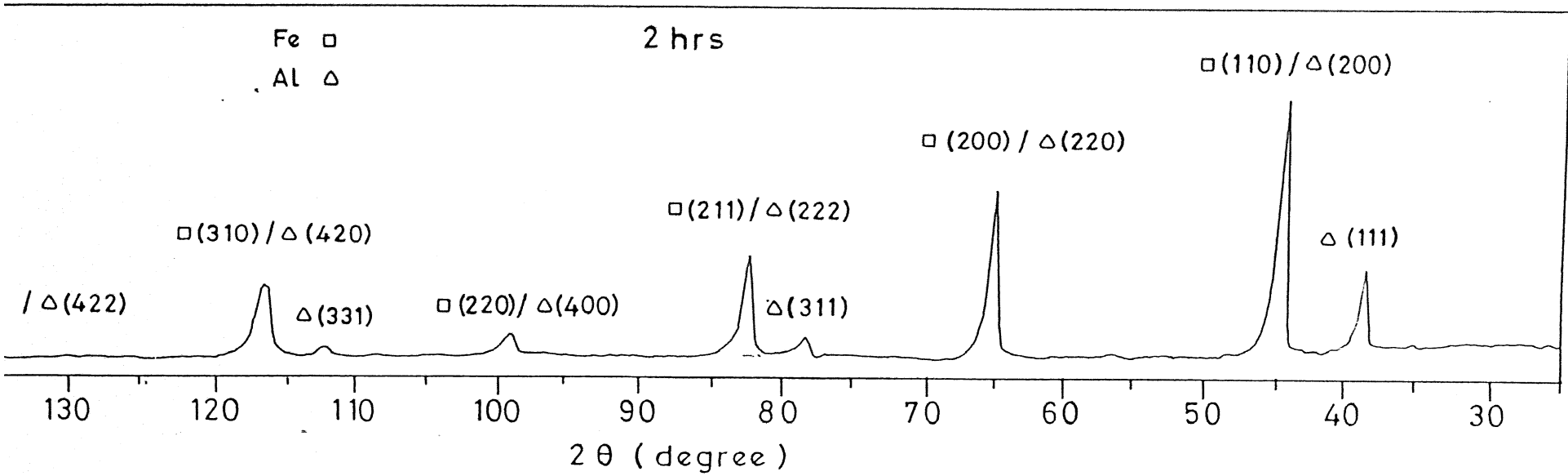

Figure 3.1: (a) X-ray Diffraction Patterns for Fe-Al-Cr powder milled for 2 hrs.

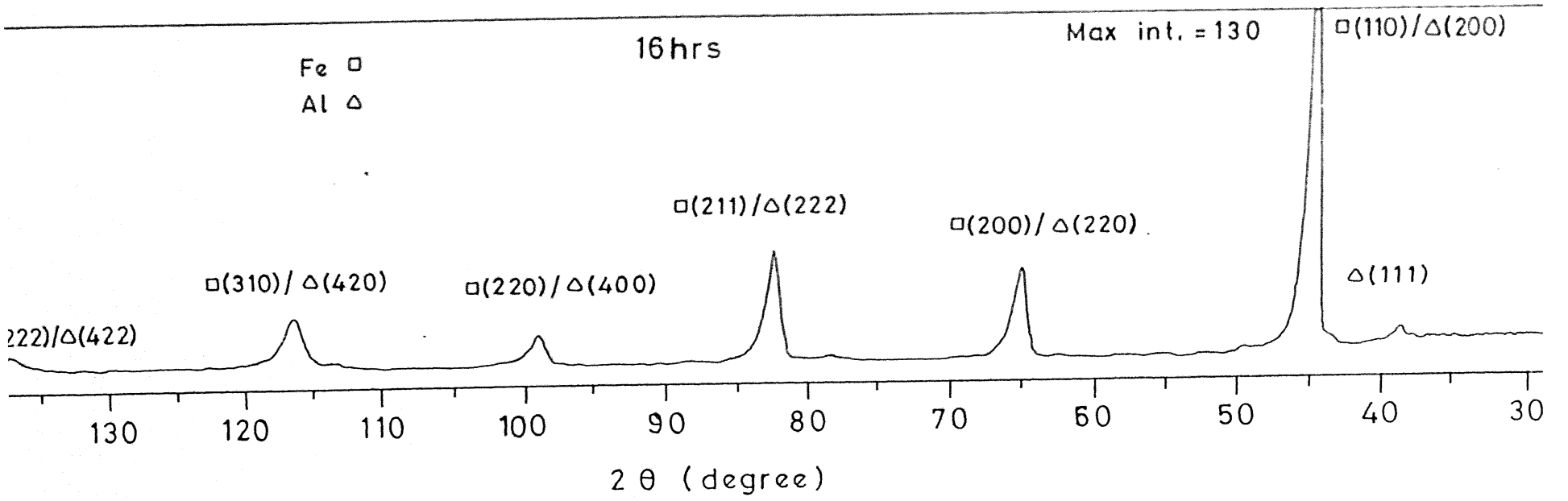

Figure 3.1: (b) X-ray Diffraction Patterns for Fe-Al-Cr powder milled for 16 hrs.

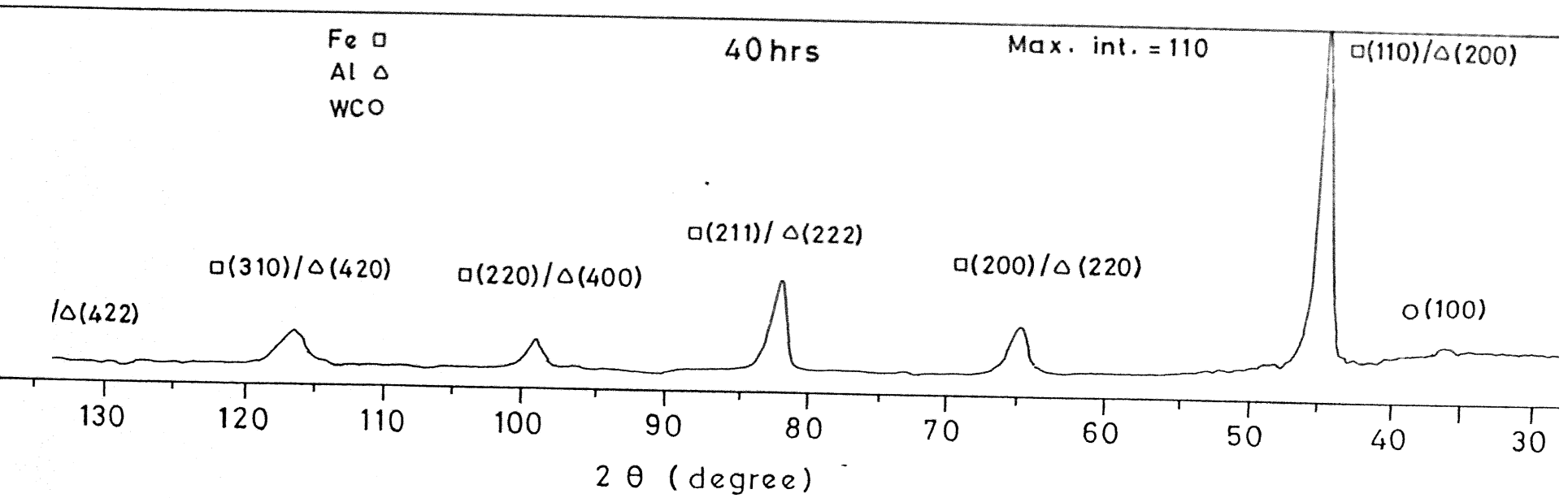

Figure 3.1: (c) X-ray Diffraction Patterns for Fe-Al-Cr powder milled for 40 hrs.

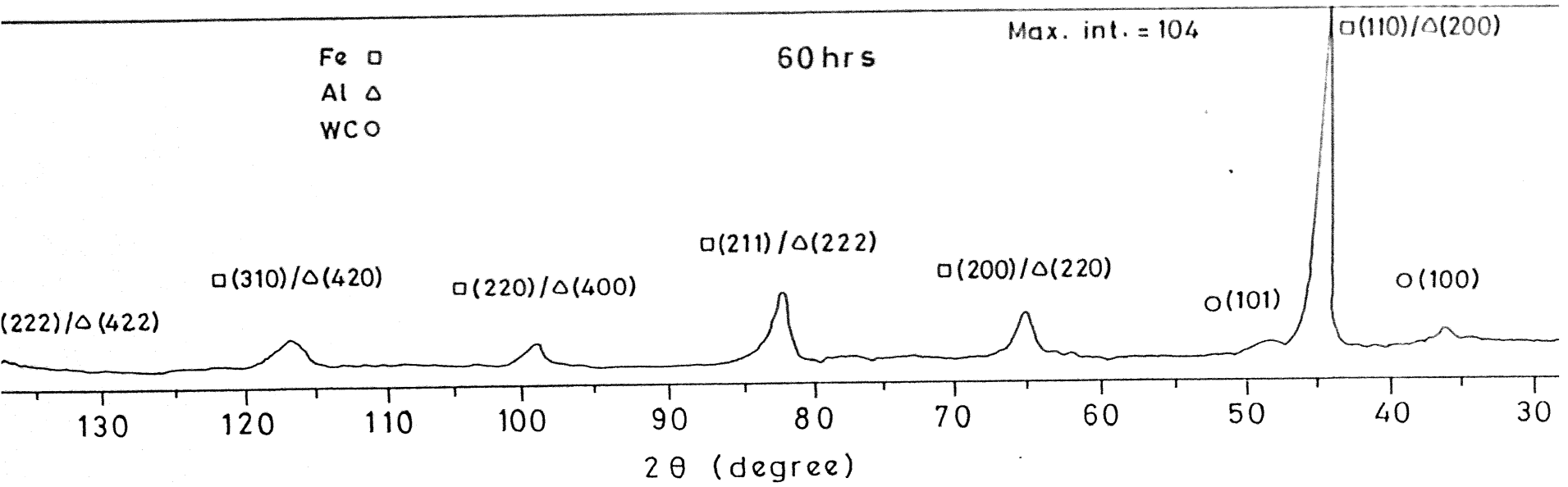

Figure 3.1: (d) X-ray Diffraction Patterns for Fe-Al-Cr powder milled for 60 hrs.

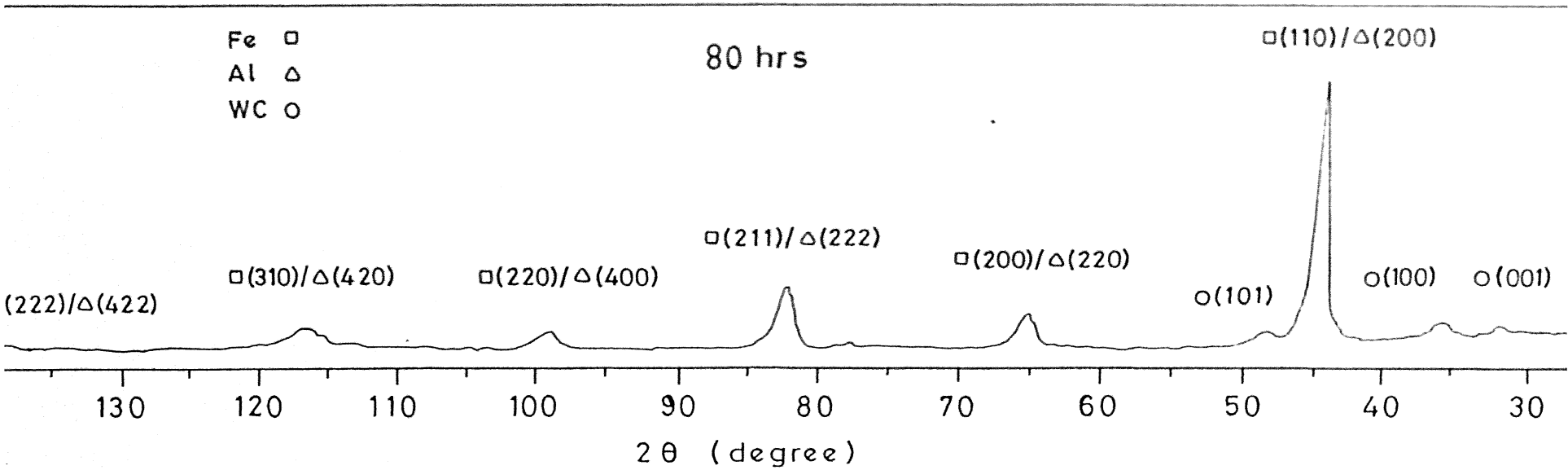

Figure 3.1: (e) X-ray Diffraction Patterns for Fe-Al-Cr powder milled for 80 hrs.

Table 3.1

Standard Data for X-ray Diffraction
for Different Elements/Compounds

Element/ Compound	(hkl)	I/I_{max}	2θ (degree)
Fe	(110)	100	44.67
	(200)	30	82.32
	(211)	20	65.02
Al	(111)	100	38.47
	(200)	47	44.74
	(311)	24	78.22
	(220)	22	65.13
Cr	(110)	100	44.37
	(211)	30	81.72
	(310)	20	115.25
Fe_3Al	(220)	100	44.41
	(422)	90	81.58
	(400)	80	64.24
	(440)	70	98.19
FeAl	(110)	100	44.2
	(211)	25	81.3
	(200)	14	64.3
	(310)	9	114.5
	(220)	8	97.6
Al_3Fe	(662)	n.a.*	43.3
	(004)	n.a.	44.8
Al_5Fe_2	(002)	n.a.	42.8
	n.a.	n.a.	44.2
	n.a.	n.a.	43.8
Al_2Fe	n.a.	n.a.	44.2
	n.a.	n.a.	44.6
	n.a.	n.a.	43.5
WC	(100)	100	35.6
	(101)	100	48.3
	(001)	45	31.5

* n.a. = not available

with Fe or Cr.

From Fig. 3.1, it can be observed that after 2 hrs of milling peaks corresponding to (111), (311) and (331) planes of elemental Al are present, but with the progress of time, these peaks got reduced in intensities. After 40 hrs. of milling, there was no trace of elemental Al left in the powder. Because peak from (111) plane of elemental Al which corresponds to 100% intensity in standard data (Table 3.1) must be present if there is any elemental Al left in the powder. It was also observed that after 32 hrs of milling tungsten carbide (WC) peaks appeared (Fig. 3.1(c)). The WC contamination of the powder during milling arose from erosion of the WC grinding balls which were used as milling media. It indicates that with the progress of milling, WC contamination increased. Initially, only peak corresponding to (100) plane of WC appeared (Fig. 3.1 (c)), and after 80 hrs. of milling peaks corresponding to (101) and (001) planes of WC were also observed (Fig. 3.1(e)). It indicates that with the progress of milling, WC contamination increased.

So, it was concluded that mechanical alloying could be completed after 40 hrs of milling for Fe-28at% Al-5at% Cr composition for 12:1 ball to charge ratio in the mechanical attritor, rotating at a speed of 500 rpm.

3.1.2 Effect of Milling Time on Crystallite Size and R.M.S. Strain

With the progress of milling, the broadening of the peaks was also observed (Fig. 3.1). The observed broadening of the diffraction lines was attributed to the refinement of the crystal size and an increase in internal strain. As discussed in Chapter 1, during mechanical alloying in a high energy mill, repeated

fracturing and cold-welding of powder particles occurs. During the early stage of the process, particles are rather soft and the welding of powder particles predominates. With the progress of milling, the powder particles get harder and harder due to extensive plastic deformation taking place during mechanical alloying, and this leads to an increased tendency for particle fracture. Therefore, crystal size becomes finer and the strain in the lattice increases with increasing milling time.

Now, to determine the crystallite size and r.m.s. strain, the approach of Williamson and Hall was used[32], which is described below:

The strain e in a crystal lattice produce some broadening B_e of the diffraction lines is given by

$$B_e = 2A \langle e^2 \rangle^{1/2} \tan \theta$$

where θ is the bragg angle, A is a coefficient which depends on the distribution of strains and close to unity for dislocation, and $\langle e^2 \rangle^{1/2}$ is the r.m.s. strain.

The broadening resulting from small crystallite size is given by the Scherrer relationship

$$B_D = \frac{K\lambda}{D \cos \theta}$$

where λ is the x-ray wave length, K is the Scherrer constant, D is the crystallite size and θ is the bragg angle.

In reciprocal space, the two components contributing to line broadening can be written as $B_e^* = A \langle e^2 \rangle^{1/2} s$ and $B_D^* = 1/D$ respectively, where $s = 2\sin \theta/\lambda$ and the Scherrer constant has been set equal to unity. By plotting the measured broadening as a function of s, the mean crystallite size D can be obtained from

the ordinate intercept and the r.m.s. strain $\langle e^2 \rangle^{1/2}$ from the slope.

Broadening is calculated by using the following formula:

$$\text{Broadening} \quad B = \sqrt{\omega_M^2 - \omega_{Fe}^2}$$

where ω_M is the peak width of milled powder of the diffraction line at any given angle which corresponds to the peak width at half of the maximum intensity. ω_{Fe} is the peak width of Fe powder for that angle.

Now, the values of $\frac{\beta \cos \theta}{\lambda}$ and $s = \frac{2 \sin \theta}{\lambda}$ were calculated for different angles for a milled powder taken out after a particular time. Now, by plotting the $\beta \cos \theta/\lambda$ on y-axis and $2 \sin \theta/\lambda$ on X-axis, we got a straight line which was drawn by best fit method. The inverse of intercept of line on y-axis gives the value of crystallite size D (since $D = \frac{\lambda}{\beta \cos \theta}$) and the slope of the straight line gives r.m.s. strain $\langle e^2 \rangle^{1/2}$.

The values of crystallite size and r.m.s. strain were calculated for all powder samples taken out after different intervals of time. The calculated values of crystallite size and r.m.s. strain were plotted against milling time which are shown in Fig. 3.2 and 3.3. respectively. It was observed from these figures that rate of refinement of crystallite decreased gradually with milling time and approached to a value of 10.83 nm after 80 hrs of milling. The r.m.s. strain was observed to increase gradually with milling time and finally reached to a value of 0.34% after 80 hrs of milling.

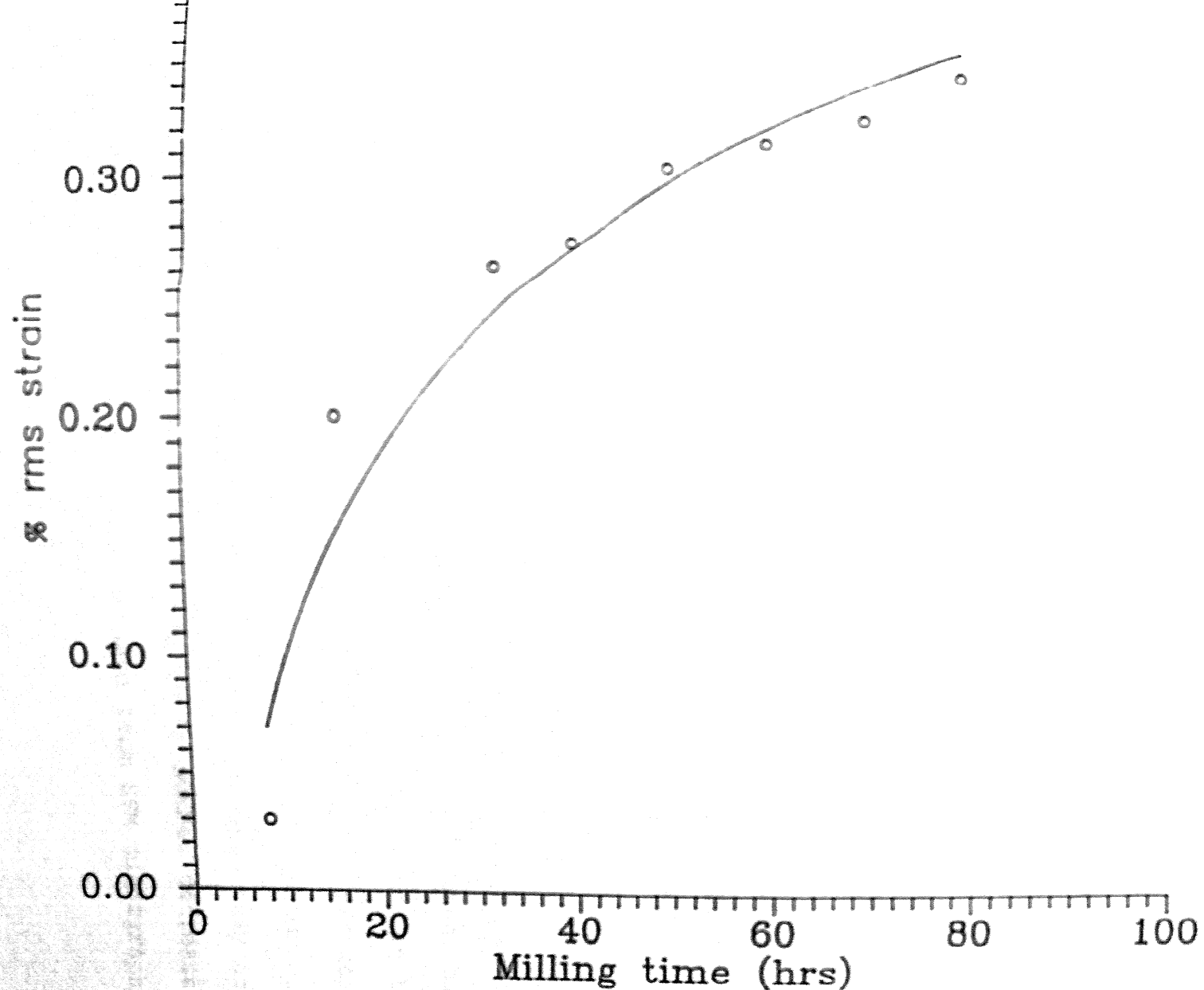

Figure 3.3: Effect of Milling Time on R.M.S. Strain.

The powder morphology and particle size were observed by SEM for powder samples taken out after 2 hrs, 16 hrs, 40 hrs, 60 hrs and 80 hrs. The SEM micrographs are shown in Fig. 3.4.

The powder morphology at any particular stage of mechanical alloying is very hard to predict because mechanical alloying in a high energy mill involves extensive deformation of particles throughout the milling. So its morphology changes very widely with time and from particle to particle. However, almost nodular morphology could be obtained after very long hours of milling.

SEM micrograph of powder samples after 2 hrs and 16 hrs of milling, exhibit a mixed morphology (Fig. 3.4 (a & b)). After 40 hrs of milling a flaky morphology can be observed (Fig. 3.4(c)). Particles of 60 hrs. milled powder also exhibit a mixed morphology (Fig. 3.4(d)). The agglomerated welded nodules can be observed in 80 hrs. milled powder. Generally, powder particles exhibit an irregular morphology in all powder samples.

Similarly, particle size of the powder sample is also very difficult to predict. A large range in the particle size can be observed in all SEM micrographs. However, it can be observed that larger particles decreases in number, and particles tends to be finer with increasing milling time. As stated earlier, particle hardness increases with milling time, and larger particles are more likely to incorporate flaws and to break apart when they are struck by the tungsten carbide balls, so their number decreases with time. Fracturing mode can also be seen from SEM micrographs (Fig. 3.4).

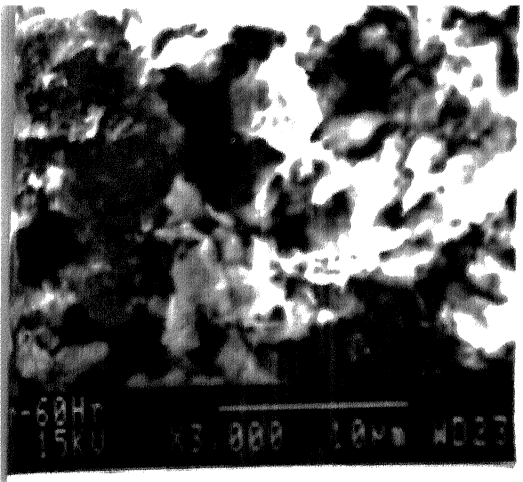
-60Hr
15KV
X3,000 10µm WD23

(d)

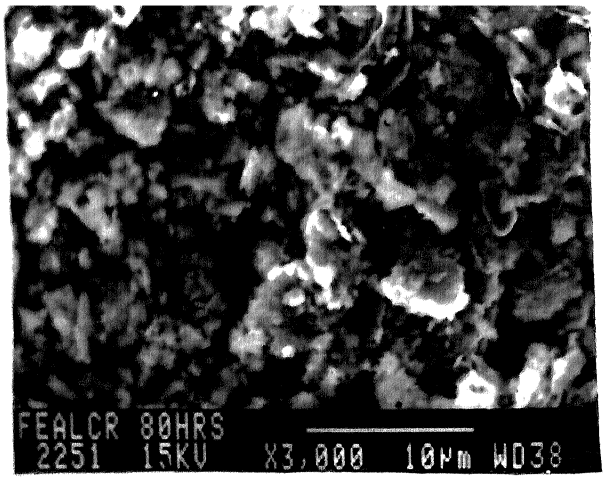
FEALCR 80HRS
2251 15KV X3,000 10µm WD38

(e)

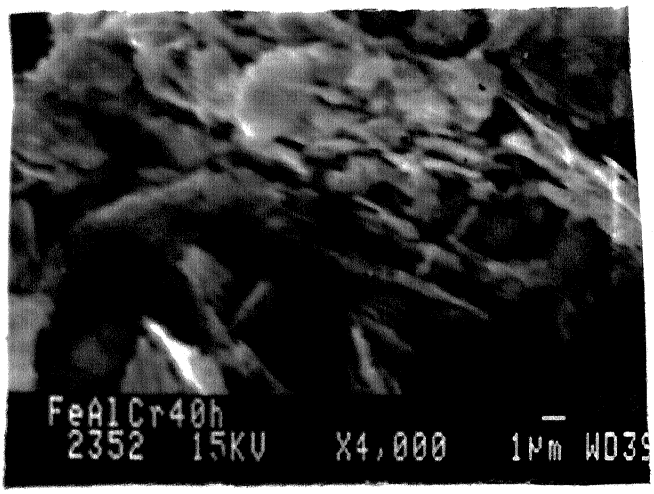
FeAlCr40h
2352 15KV X4,000 1µm WD39

(c)

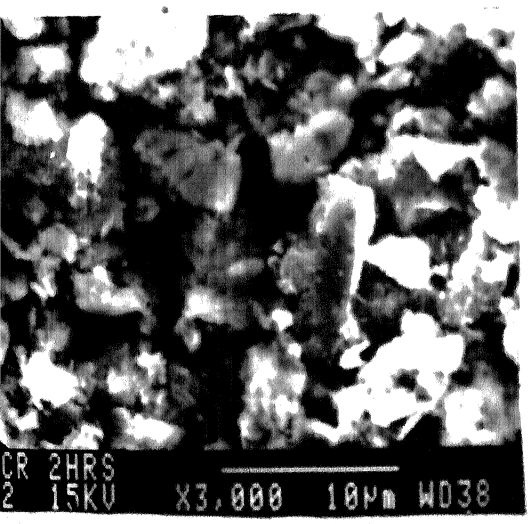
CR 2HRS
2 15KV X3,000 10µm WD38

(a)

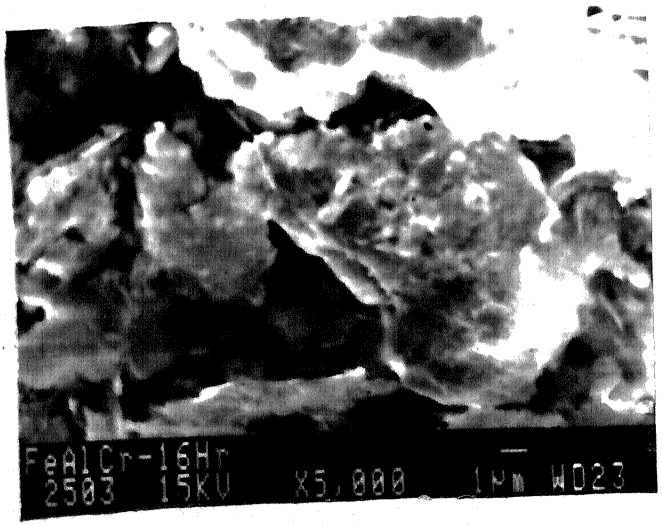
FeAlCr-16Hr
2503 15KV X5,000 1µm WD23

(b)

ar

3.2 COLD COMPACTION, SINTERING AND HOT ROLLING OF MECHANICALLY ALLOYED POWDER

3.2.1 Effect of Cold Compaction on Mechanically Alloyed Powder

The powder obtained after 80 hrs. of milling was dried in oven at 40°C to evaporate acetone completely from the powder. Then, the compacts of 31 mm diameter were made by cold compaction as discussed in Chapter 2.

3.2.1.1 *Effect of Cold Compaction on Green Density*

The green density and porosity of all compacts made at three different compaction pressures are shown in Table 3.2. The maximum green density (2.84 gm/cc) which was achieved after applying maximum compaction pressure (318 MPa) was very low compared to theoretical density of the powder (theoretical density was assumed to be that of Fe_3Al intermetallic, i.e. 6.69 gm/cc). The low green density of the compacts made by cold compaction could be attributed to the very high hardness of the mechanically alloyed powder which has been discussed earlier. Generally, consolidation of mechanically alloyed powder by cold compaction to achieve sufficient green density, is done by applying a very high pressure (~ 3 GPa)[33]. This pressure is nearly 10 times more than the maximum pressure that can be applied in this case. Also, due to WC contamination which itself is a very hard material, the compaction pressure needed to achieve high green density may rise further.

3.2.2 Effect of Sintering on Green Compacts

To achieve sufficient compact density, sintering of the green compacted samples were performed at 1100°C for 1/2 hrs and 2 hrs in argon atmosphere as discussed in Chapter 2.

Table 3.2

Densities of Green Compacts at Differnt Pressures

Shape : Cylindrical Compacts
Dia : 31 mm
Avg. Thickness : 7.96 mm

ompaction ressure	Sample Identity	Green Density (gm/cc)	% Porosity
	1	2.43	63.7
97 MPa	2	2.15	67.9
	3	2.25	66.4
	4	2.46	63.2
195 MPa	5	2.61	61.0
	6	2.52	62.3
	7	2.84	57.5
	8	2.67	60.0
318 MPa	9	2.74	59.0
	10	2.72	59.3
	11	2.76	58.7

3.2.2.1 *Density of Sintered Compacts*

After sintering, sintered density of all compacts were measured by the method discussed in Chapter 2. The % porosity and % volume shrinkage during sintering for all compacts were also calculated. The results, thus, obtained are shown in Table 3.3.

Maximum sintered density obtained was 4.46 gm/cc after 1/2 hrs of sintering at 1100^{o}C. No significant change in sintered density was observed after two hours of sintering. Maximum sintered density (4.46 gm/cc) was 67% of theoretical density, which was obtained for maximum green compact density (2.84 gm/cc). Higher sintering temperature as well as higher green density may lead to higher sintered density[34].

3.2.2.2 *Microstructural Features of Sintered Compacts*

A large number of pores in the sintered compact can be seen from SEM micrograph of a sintered compact, shown in Fig. 3.5. Inter connected porosity was observed. Rounding of the pores were also observed as can be seen in Fig. 3.5.

3.2.2.3 *Hardness of Sintered Compacts*

The microhardness of all compacts were also measured and shown in Table 3.4. The high microhardness of the sintered compacts may be attributed to the high hardness of the mechanically alloyed powder. The maximum microhardness obtained was 675 HV which corresponds to the compact of maximum sintered density (4.46 gm/cc). The microhardness was found to increases with increasing sintered density.

The Rockwell hardness of the sintered compacts were also tried to measure but all samples failed in a brittle manner when tried to test on C scale i.e. on an applied load of 150 kg. Also,

Table 3.3

Densities of Sintered Compacts

Sample Identity	Sintering Time (hrs)	Green Density (gm/cc)	Sintered Density (gm/cc)	% Porosity	% Volume Shrinkage
1	1/2	2.43	3.59	46.3	42.2
2	1/2	2.15	4.02	39.9	50.4
3	1/2	2.25	3.65	45.4	47.3
4	1/2	2.46	4.02	39.9	49.8
5	1/2	2.61	3.67	45.1	37.8
6	1/2	2.52	4.03	39.8	45.3
7	1/2	2.84	4.46	33.3	35.4
8	1/2	2.67	3.70	44.6	36.6
9	1/2	2.74	3.92	41.4	40.8
10	2	2.72	3.78	43.5	30.3
11	2	2.76	3.80	43.2	31.0

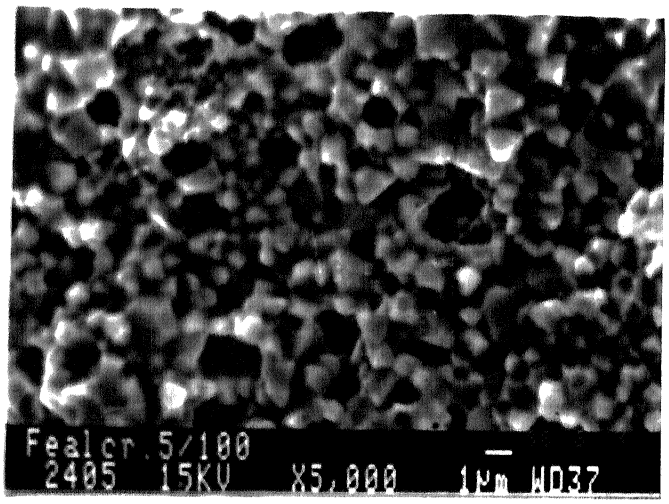

Figure 3.5: SEM Micrograph of Sintered Compact.

Table 3.4

Microhardness of Sintered Compacts

Sample Identity	Microhardness (HV)	Sintered Density (gm/cc)
1	546	3.59
2	598	4.02
3	562	3.65
4	615	4.02
5	579	3.67
6	625	4.03
7	675	4.46
8	580	3.7
9	630	3.92
10	598	3.78
11	604	3.80

no impression could be made when lower loads (of 50 kg and 100 kg) were applied due to high strength of the material.

3.2.2.4 *Compressive Strength of Sintered Compacts*

The compression testing was also performed for compacts and the results are shown in Table 3.5. The compressive strength until failure was found to be 543 MPa and 528 MPa for compacts of sintered densities 3.78 and 3.59 respectively. The compressive strength of the Fe-28%Al-2%Cr compacts made by mechanical alloying of prealloyed powder and their subsequent processing by shock consolidation is reported in literature as around 2.1 GPa[35]. The low compressive strength could be attributed to the very high porosity in sintered compacts.

3.2.2.5 *Electron-Probe Microanalysis of Sintered Compacts*

Electron Probe Micro-Analysis of a sintered compact is shown in Table 3.6. A high percentage of W in compact was observed. Generally, an overall high percentage of Fe was observed at all points. A solid solution of Al in Fe may be expected to form.

3.2.3 Effect of Hot Rolling on Sintered Compacts

Since, sintered compacts had lower densities, so to get nearly full density compacts, hot rolling of sintered compacts were also tried at 1100^{o}C and the soaking time of the compact was 30 min. But, due to very brittle nature of the compacts, hot rolling was not successful and compact fractured in a brittle manner during hot rolling.

3.3 HOT PRESSING OF MECHANICALLY ALLOYED POWDER

Hot pressing of the 80 hrs. mechanically alloyed powders was done at four different temperatures of 800^{o}C, 900^{o}C, 1000^{o}C and 1100^{o}C at a constant pressure of 20 MPa. The holding time was

Table 3.5

Compressive Strength of Sintered Compacts

Sintered Density (gm/cc)	Compressive Failure Strength (MPa)
3.78	543
3.59	528

Table 3.6

Electron Probe Micro-analysis of Sintered Compacts

Point		Element			
		Fe	Al	Cr	W
Point 1	wt %	67.31	26.66	3.35	2.68
	atom %	53.04	43.48	2.84	0.64
Point 2	wt %	66.02	27.48	3.30	3.2
	atom %	51.81	44.65	2.78	0.76
Point 3	wt %	57.44	36.80	5.72	0.04
	atom %	41.09	54.50	4.40	0.01
Point 4	wt %	68.13	28.76	2.65	0.46
	atom %	52.15	45.56	2.18	0.11

kept as 5 and 15 minutes.

3.3.1 Effect of Hot Pressing on Mechanically Alloyed Powder

3.3.1.1 *Density of Hot Pressed Compacts*

The density and porosity of the all hot pressed compacts were calculated and are shown in Table 3.7. It was observed that maximum density of the hot pressed compacts was 6.27 gm/cc at 1000^{o}C and 15 min. holding time. It was also observed that for the same holding time, density increased with temperature. So higher densification could be achieved at higher temperatures if holding time was kept constant. It was also observed that holding time plays an important role in densification during hot pressing. Maximum densification was obtained at 1000^{o}C and not at 1100^{o}C, because holding time was longer at 1000^{o} temperature. Therefore, densification during hot pressing depends on temperature as well as on holding time. Densification is very high in hot pressed compacts compared to sintered compacts.

3.3.1.2 *Microstructural Features of Hot Pressed Compacts*

The SEM micrographs of a hot pressed samples for unetched and etched conditions are shown in Fig. 3.6(a & b) respectively. The unetched sample seemed to consist of two regions (black & white) But etching of the same sample revealed that the black region was nothing but fine porosity. The porosity was very fine and less compared to sintered compacts.

3.3.1.3 *Hardness of Hot Pressed Compacts*

The microhardness of the all hot pressed samples are shown in Table 3.8. The microhardness was found to be more for higher density compact. The maximum microhardness obtained was 1050 HV which corresponds to the compact of maximum density (6.27 gm/cc).

Table 3.7

Densities of Hot Pressed Compacts

Pressure applied = 20 MPa

Temp (^{o}C)	800	900	1000	1100	1100
Holding Time (min)	15	5	15	5	5.
Density (gm/cc)	4.96	3.64	6.27	6.03	6.05
% Porosity	25.9	45.6	6.3	9.9	9.6

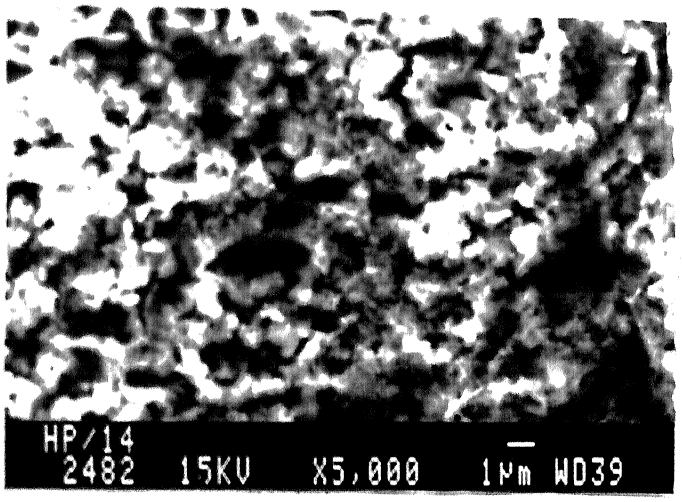

(b)

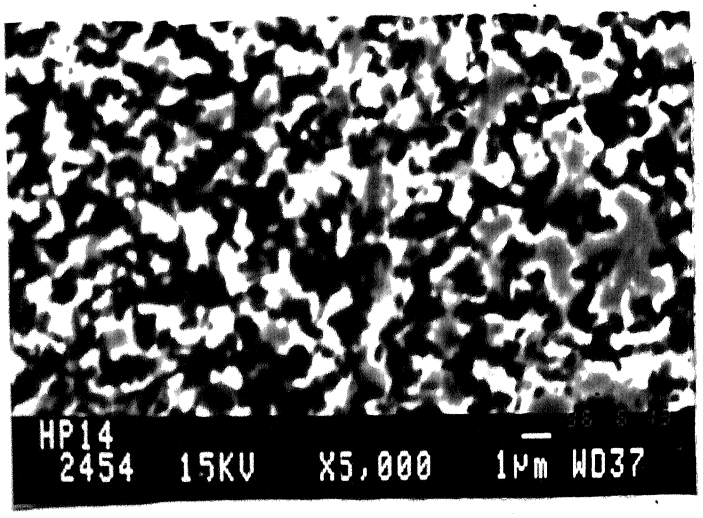

(a)

Figure 3.6: SEM Micrographs of Hot Pressed Compacts (a) Unetched and (b) Etched.

Table 3.8

Hardness of Hot Pressed Compacts

Temp (^{o}C)	800	900	1000	1100	1100
Density (gm/cc)	4.96	3.64	6.27	6.03	6.05
Microhardness (HV)	563	363	1050	963	967
Rockwell Hardness (R_c)	-	-	62	54	-

The microhardness of the hot pressed compacts are more compared to sintered compacts. This could be attributed to higher densities (i.e. less porosity) of hot pressed compacts.

The Rockwell hardness on C scale of the compacts hot pressed at 1000^{o}C and 1100^{o}C were found to be 62 Rc and 54 Rc respectively. The compacts hot pressed at 800^{o}C and 900^{o}C broke during Rockwell hardness testing due to high porosity.

3.3.1.4 *Compressive Strength of Hot Pressed Compacts*

During compression testing of compact, hot pressed at 1100^{o}C, it was found that compact did not fail even after applying an stress of 1.89 GPa and no evidence of plastic deformation was found even after applying such a high stress. It indicates that hot pressed material has a very high compressive strength compared to those reported in literature[34] and also higher than those of sintered compacts.

CHAPTER 4

CONCLUSIONS

Based on the results of present investigations on mechanical alloying, cold compaction and sintering of mechanically alloyed powder and hot pressing of mechanically alloyed powder, the following conclusions can be drawn:

1. Mechanical alloying of chromium containing Fe - Al powder could be completed after 40 hours of milling for Fe-28at%Al-5at%Cr. composition for 12:1 ball to charge ratio in a high energy in mechanical attritor, rotating at a speed of 500 rpm and a solid solution of Al and Cr in Fe was formed.
2. Nano crystalline size was obtained after 80 hours of mechanical alloying, also r.m.s. strain was found to increase with the progress of time during high energy attritor milling.
3. Cold compaction of mechanically alloyed powder and its subsequent sintering does not seem to be a viable powder metallurgical processing route to produce high density compacts with superior mechanical properties.
4. Hot pressing of mechanically alloyed powder seems to be a feasible processing route to achieve high density. The density of the hot pressed compact increases with increasing temperature for a constant holding time at a given pressure. The density also increases with increasing holding time for a

given temperature and at a given pressure.

5. Mechanical properties of hot pressed compacts are superior than those of sintered compacts.

6 Hot pressing seems to be more viable route for processing of mechanically alloyed Fe-Al-Cr powder than cold compaction and sintering route.

REFERENCES

C.T. Liu and J.O. Stiegler, "Ordered Intermeta Properties and Selection: Non-ferrous alloys and purpose materials, Metals Handbook, vol. 2, 10th ed International, 1990, p. 913.

N.S. Stoloff, Ordered alloys-physical metallurgy structural applications, International Metals Reviews, Vol. 29, No. 3, p. 123.

C.T. Liu and K.S. Kumar, "Ordered Intermetallic Alloys; I: Nickel and Iron Aluminides", JOM, May, 1993, p. 38.

C.T. Liu and K.S. Kumar, "Ordered Intermetallic Alloys, II, Sillicides, trialuminides and others", JOM, June 199 28.

K. Oki, M.Hasaka and T.Eguchi, "Process of Order-Dis Transformation in Iron-Aluminium Alloys", Japanese Journa Applied Physics, Vol. 12, No. 10, October, 1973, p. 1522.

S.M. Allen, J.W. Cahn, "Mechanism of P Transformation within the Miscibility gap of Fe-rich Fe alloys", Acta. Metall. 24 (1976), p. 425.

K. Ho and R.A. Dodd, "Point defects in FeAl", Scr. Metall. Vol. 12, 1978, p. 1055.

U. Prakash, R.A. Buckley, H. Jones and C.M. Sellars, "Structure and properties of ordered intermetallics based on the Fe-Al system", ISIJ International, Vol. 31, 1991, No. 10, p. 1113.

C.G. McKamey, J.A. Horton and C.T. Liu, "High Temperature Ordered Intermetallic Alloys II", ed. by N.S. Stoloff, C.C. Koch and O. Izumi,C. T.Liu, MRS Symp. Proc., Vol. 81, MRS, Pittsburgh (1987), p. 321.

H. Inouye, "High Temperature Ordered Intermetallic Alloys", MRS Symp. Proc., ed. by C.C. Koch, C.T. Liu and N.S. Stoloff., MRS, Pittsburgh, PA, 1985, 39, p. 255.

R.S. Diehm and D.H. Mikkola, "High Temperature Ordered Intermetallic Alloys II", ed by N.S. Stoloff,C.C.Koch,C.T.Liu,O.Izumi , MRS, Symp. Proc., Vol. 81, MRS, Pittsburgh, 1987, p. 329.

J.D. Whittenberger; "The influence of grain size composition on slow plastic flow in FeAl between 1100 to K". Mat.Sci.& Engg. , Vol. 77, 1986, p. 103.

3. D.G. Morris,M.Nazmy,C.Noseda , "Creep Resistance in a New Alloy Based on Fe_3Al", Scripta Metallurgica et Materiallia, Vol. 31, No. 2, p. 173, 1994.

4. I. Jung,M.Rudy,G.Sauthoff , "High Temperature Ordered Intermetallic Alloys II, ed. by N.S. Stoloff,C.C.Koch,O.Izumy,C.T.Liu, MRS Symp. Proc., Vol. 81, MRS. Pittsburgh (1987), p. 321.

5. Z. Zhonghua,S.Yanashan,G.Jun, "Effect of Niobium Addition on the Mechanical Properties of Fe_3Al based Alloys", Scripta Metallurgica et. Materialia, Vol. 33, No. 12, 1995, p. 2013.

6. N.S.Stoloff,G.E.Fuchs,A.K.Kuruvilla,S.Choe, " High Temperature Ordered Intermetallic Alloys II", ed. by N.S.Stoloff,C.C.Koch,O.Izumy,C.T.Liu, MRS Symp. Proc., Vol. 81, MRS, Pittsburgh, 1987, p. 247.

7. X. Wang,J.V.Wood, "Role of Nickel in Fe_3Al Intermetallic Compound Formation", Powder Metallurgy, Vol. 38, No. 1, 1995, p. 59.

8. S. Yangshan,Y.Zhengjun,Z.Zhonghua,H.Haibo, "Mechanical Properties of Fe_3Al Based Alloys with Cerium Addition", Scripta Metallurgica et. Materiallia, Vol. 33, No. 5, 1995, p. 811.

9. W.R.Kerr, "Fracture of Fe_3Al", Metallurgical Transactions, Vol. 17A, Dec. 1986, p. 2298.

10. V.K. Sikka, C.G. Mckamey, S. Viswanathan, "Development and Commercialization Status of Fe_3Al-based intermetallic Alloys", in Structural Intermetallics, ed. by C.T. Liu, N.S. Stoloff, C.C. Koch, the Mineral, Metals & Materials Society, 1993, p. 483.

11. P. Johansson, B. Uhrenius, A. Wilson, U. Stahlberg, "Processing, Fabrication and Mechanical Properties of Fe_3Al based PM alloys", Powder Metallurgy, Vol. 39, No. 1, 1996, p. 53.

12. B.H. Rabin, R.N. Wright, "Synthesis of Iron Aluminides from elemental powders, reaction mechanism and densification behaviour", Meta. Trans., Vol. 22A, Feb. 1991, p. 277.

13. B.J.M. Aikin, T.H. Courtney, "The Kinetics of Composite Particle Formation during Mechanical Alloying", Met. trans., Vol. 24A, Mar. 1993, p. 647.

14. J.S. Benjamin, "New Materials by Mechanical Alloying Technique", ed. by E. Arzt & L. Schultz, 1989, p. 3.

25. D.R. Maurice, T.H. Courtney, "The Physics of Mechanical Alloying", Met. Trans., Vol. 21 A, Feb. 1990, p. 289.

26. C. Suryanarayana, F.H. Froes, D.K. Mukhopadhyay,G. Cizmich, G.H. Chen, Z. Peng, J, Mishurda, "Synthesis of Intermetallics by Mechanical Alloying", Processing and Fabrication of Advanced Materials III, Ed. by V.A. Ravi, T.S. Srivaisan, J.J. MooraThe Minerals, Metals and Materials Society, 1994, p. 567.

27. R.B. Schwarz, "Introduction to the Viewpoint set on, Mechanical Alloying", Scripta, Materiallia, Vol. 34, No. 1, 1996, p. 1.

28. G.H. Fair, J.V.Wood, "Mechanical Alloying of Iron-Aluminium Intermetallics", Powder Metallurgy, Vol. 36, No. 2, 1993, p. 123.

29. D.G. Morris, M.A. Morris, "Mechanical Intermixing and alloying of intermetallics", World Conference on Powder Metallurgy, 2-6 July, 1990, Wembley Conf. Lenb, London, Vol. 2, p. 47.

30. D. Oleszak, P.H. Shingu, "Mechanical Alloying in the Fe-Al System", Materials Science and Engg., A 181/A 182 (1994), p. 1217.

31. E.C. Deane and R.F. Cochrane, "Effect of Process Variables on the Mechanical Alloying of Iron Aluminide".(Conference Paper).

32. G.K. Williamson & W.H.Hall, "X-ray Line Broadening from Filed Aluminium and Wolfrom", Acta, Meta., Vol. 1, Jan. 1953, p. 26.

33. E.Y. Gutmonus, "New Materials by Mechanical Alloying Techniques", ed. by Arzt & Schultz, Calw-Hirsaw (FRG), Oct. 1988, p. 129.

34. D.Q. Yi, C.H. Li, J.H. Wang, R. Warren and I. Olefjord, "Preparation of Fe_3Al based iron aluminides from elemental and prealloyed powders", Materials Science & Technology, July 1995, Vol. 11, p. 680.

35. M. Jain & T. Christman, "Synthesis, Processing, and Deformation of Bulk Nanophase Fe-28Al-2Cr Intermetallic", Acta Metall. Mater., Vol. 42, No. 6, 1994, p. 1901.

36. L. Lu & M.O. Lai, "Formation of New Materials in the Solid State by Mechanical Alloying", Materials & Design, Vol. 16, No. 1, 1995, p. 33.

37. R. W. Rudin, D. Maurice, T.H. Courtney, "Milling Dynamics, Part I, Attritor Dynamics", Results of a Cinematographic Study", Met. Trans., Vol. 24A, Jan. 1993, p. 175.

38. R.G. Baligidad, U. Prakash, V.R. Rao, P.K. Rao, N.B. Ballal,"Development of Fe_3Al Based Intermetallic Alloys by Electroslag Remelting", ISIJ International, Vol. 35, 1995, No. 4, p. 443.

39. I. Baker, H. Xiao, O. Klein, C. Nelson, J.D. Whittenberger, "The Effect of Temperature and Fe: Al Ratio on the Flow and fractures of FeAl", Acta Metall. Mater, Vol. 43, No. 4, 1995, p. 1723.

40. K. Oki, M. Hasaka, T. Eguchi, "An X-ray Diffraction Study of Kinetic Behaviours of Ordering in Fe_3Al Alloys", Journal of Japan Institute of Metals, Vol. 35, 1971, p. 919.

41. R. J. Lynch and L.A. Heldt, "Effects of Annealing temperature on the Mechanical Properties of an Fe-36 % Al Alloy", Scripta Meta. et. Mater., Vol.30, No. 7, 1994, p. 895.

42. M.G. Mendiratta, H. Kim, H.A. Lipsitt, "Slip Directions in B2 Fe-Al Alloys", Met. Trans., Vol. 15A, Feb. 1984, p. 395.

43. C.H. Kong & P.R. Munroe, "The Effect of Ternary Additions on the Vacancy Hardening of FeAl", Scripta Met. et. Mate, Vol. 30, No. 8, 1994, p. 1079.

44. H. Okamoto & P.A. Beck, "Phase Relationships in the Iron-Rich Fe-Al Alloys", Met. trans., Vol. 2, Feb. 1971, p. 569.

45. C. Suryanarayana, G.H. Chen, F.H. Froes, "Milling maps for phase Identification during Mechanical Alloying", Scrip. Meta. et. Mater., Vol. 26, No. 11, p. 1727.

46. K. Oki, H. Sagane, T. Eguchi, "Electron Microscopic Study of Domain Structure in Fe-Al Alloys", Japanese Journal of Applied Physics, Vol. 13, No. 5, May 1974.

47. B.S. Murty, "Mechanical Alloying - a novel synthesis route for amorphous phases", Bull. Mater. Sci., Vol. 16, No. 1, Feb. 1993, p. 1.